Spring 4-12-2019

Incorporation of EGFR and RON Receptors into Nanodiscs

Cristina Flores-Cadengo
University of New Mexico

Follow this and additional works at: https://digitalrepository.unm.edu/bme_etds

Part of the Biological Engineering Commons, Biophysics Commons, Molecular Biology Commons, Molecular, Cellular, and Tissue Engineering Commons, Nanoscience and Nanotechnology Commons, Other Medicine and Health Sciences Commons, and the Structural Biology Commons

Cristina Flores-Cadengo

Candidate

Biomedical Engineering

Department

This thesis is approved, and it is acceptable in quality and form for publication:

Approved by the Thesis Committee:

Dr. Diane Lidke   , Chairperson

Dr. Mara P. Steinkamp

Dr. Eva Chi

Incorporation of EGFR and RON Receptors into Nanodiscs

by

Cristina Flores-Cadengo

B.S. Chemical Engineering, Instituto Tecnológico de Aguascalientes, 2016

THESIS

Submitted in Partial Fulfillment of the

Requirements for the Degree of

Master of Science

Biomedical Engineering

The University of New Mexico
Albuquerque, New Mexico

May 2019

Acknowledgements:

I would like to thank first and foremost my committee chair and mentor, Dr. Diane Lidke. I will always be grateful for the opportunity she gave me to work in a great environment that pushed me to gain knowledge and be curious. I would also like to thank my committee members: my advisor, Dr. Mara Steinkamp, whose hands-on teachings made this project possible, as well as Dr. Eva Chi who has been a huge resource and a great person.

I would like to thank Dr. Bridget Wilson for giving me the opportunity to collaborate with her and the team, as well as welcoming me into the laboratory. I would like to thank the New Mexico SpatioTemporal Modeling Center at UNM for providing the funding for this project and pushing scientific research forward.

I have been fortunate to meet and work alongside a very diverse group of intelligent and amazing people during my graduate studies at UNM. I would like to thank the members of the OWLS (Janet Oliver, Bridget Wilson, Diane Lidke, and Mara Steinkamp) lab for the knowledge you have built over the years, and your constant spirit of wonder and diligence. More specifically, I would like to thank Rachel Grattan and Dr. Sandeep Pallikkuth for their patience, help, and involvement on this project. Dr. Carolina Franco-Nitta for always being there to answer questions and offer help, whether it was or not scientifically-related. Ashley Remy for teaching me all I needed to know before I began working on this project. I would also like to thank former and current graduate students whose journey intertwined with mine and blossomed in friendship, Emanuel Salazar-Cavazos, Derek Rinaldi, and Will Kanagy. I will always be grateful for your help, your encouragement, and company. I would also like to thank Dr. Elton Jhamba for helping me familiarize with some of the microscopy equipment, as well as providing interesting conversation during imaging sessions. Shayna Lucero for her help with tissue culture and her friendship. I would like to thank every member of the lab I had the pleasure to meet for welcoming me, offering me their help, knowledge, and friendship. I would also like to thank Dr. Stanly Steinberg for putting me in contact with Dr. Bridget Wilson, had he not replied to my email I would have never met such wonderful people.

I would also like to thank Linda Bugge, as well as the professors and staff who are part of the Biomedical Engineering program. Thank you for your help, your teachings, and your work.

Incorporation of EGFR and RON Receptors into Nanodiscs

By

Cristina Flores-Cadengo

B.S. Chemical Engineering, Instituto Tecnológico de Aguascalientes, 2016

M.S. Biomedical Engineering, University of New Mexico, 2019

ABSTRACT

Understanding the structure-function relationship of membrane receptors is essential to comprehend the crosstalk between key signaling pathways. Aberrant trans-activation between receptors can lead to tumorigenesis. Two of these receptors known to be involved in cancer development are receptor tyrosine kinases (RTKs), RON (Recepteur d'Origine Nantais) and EGFR (Epidermal Growth Factor Receptor). There has been evidence of heterodimerization and crosstalk between these two receptors based on co-immunoprecipitation, however the structural requirements behind these interactions remain unknown. Structural studies could provide insights into these RTKs' modes of dimerization and structure-function relationship. However, structural studies of full-length membrane proteins are often difficult due to poor solubility of the hydrophobic transmembrane domains. This affects protein structure and functionality. The use of nanodiscs for protein structural studies helps provide a native-like environment for membrane proteins, helping to avoid denaturing and aggregation, as well as providing a homogeneous size which makes them ideal for imaging techniques. In this work, we focus on optimizing a nanodisc assembly protocol to incorporate full-length RON and EGFR receptors into nanodiscs, as well as developing techniques to detect protein incorporation into these nanodiscs, which would ultimately facilitate structural studies for RON and EGFR heterodimerization. These studies could provide a mechanistic justification for novel targeted therapies in cancer.

Table of contents

TABLE OF FIGURES

CHAPTER 1: INTRODUCTION

1.1.   Receptor Tyrosine Kinases signaling and function

Receptor Tyrosine Kinases (RTKs) are cell-surface receptors that are essential in multiple cell processes, such as metabolism, survival, proliferation, differentiation, motility, and cell cycle control (Ullrich, 1990; Blume-Jensen 2001). RTKs are single-pass transmembrane proteins that bind ligands (Maruyama, 2014). Humans have 58 known RTKs divided in 20 subfamilies with similar molecular structures (Lemmon, 2010). The general structure of an RTK consists of an extracellular ligand-binding domain, a single helix transmembrane domain, and a cytoplasmic region containing a tyrosine kinase domain as well as carboxy-terminal and juxtamembrane regulatory regions (**Figure 1**).
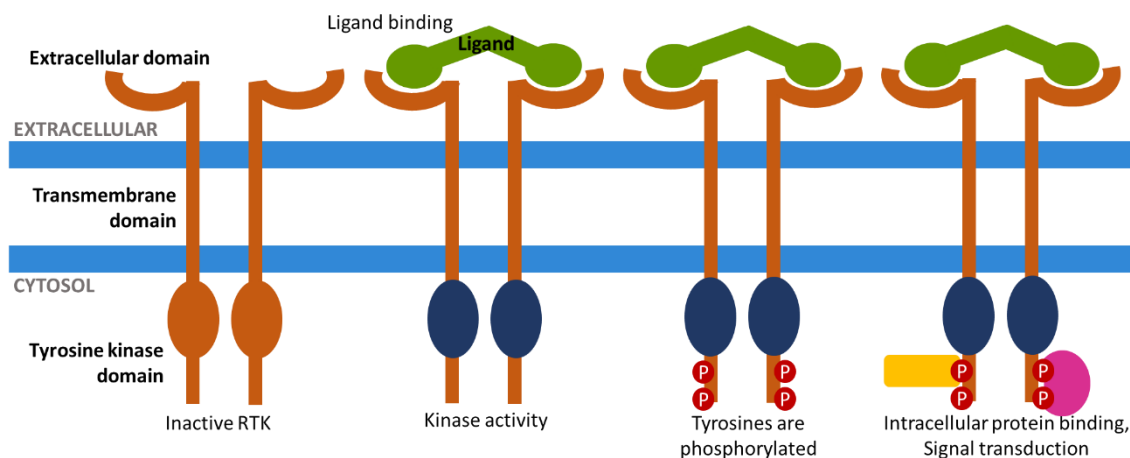
Figure 1. General RTK structure and ligand-based dimerization mode. RTK basic structure contains an extracellular ligand-binding domain, a single-pass transmembrane domain, and a tyrosine kinase domain. Upon ligand binding, kinases are activated and tyrosines are phosphorylated, which allows intracellular protein binding and triggers several signaling pathways.

Phosphorylation of the tyrosine allows for communication of extracellular information to intracellular signaling proteins. RTKs accomplish this function through activation of
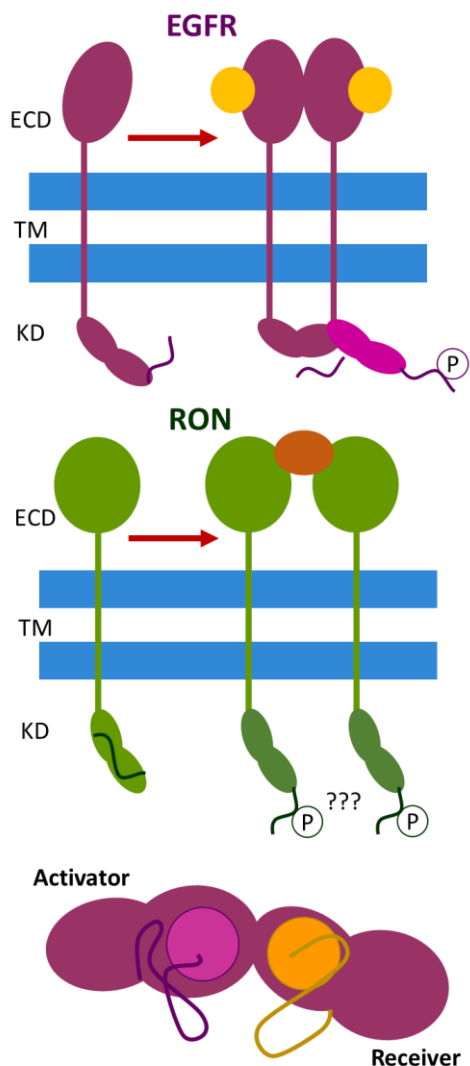
Figure 2. EGFR and RON dimerization modes. A. EGFR receptor-mediated dimerization. EGFR dimerizes through the extracellular domain after ligand binding, bringing the kinase domains (KD) together and forming an asymmetric dimer. In this case, the ligand does not form part of the interface between receptors (EGF in yellow). B. The modes or RON dimerization are not entirely known. It is thought that RON forms dimers in the absence of ligand by overlapping ECDs. The orientation of KDs upon dimerization is unknown. (MSP in orange) C. "Activator-Receiver" model for EGFR dimerization. This model establishes allosteric activation by direct contact between two KDs from two receptors. The Activator's C-lobe creates contact with the Receiver's N-lobe, destabilizing autoinhibitory interactions of the Receiver's activation loop.

their protein kinase domain. In general, one ligand binding to the extracellular domain triggers receptor dimerization and leads to activation (**Figure 2**). Association of the extracellular region guides the intracellular domains into dimeric conformation, bringing their kinase domains together in an asymmetric dimer and thus increasing kinase activity and producing phosphorylation of tyrosine residues. Some of these tyrosine residues help maintain active conformation of the kinase, while some tyrosines act as docking sites for other proteins that propagate signaling pathways (Ullrich, 1990; Lemmon 2010 Maruyama, 2014). Generally, RTK dimerization occurs when two ligand-bound monomers initiate signaling. However, some RTKs are also thought to exist as pre-formed, inactive, dimers.

There are several mechanisms of dimerization for RTK family members that involve a combination of ligand-mediated and

receptor-mediated components. Ligand-mediated interactions are the most commonly known. These occur when a bivalent ligand interacts simultaneously with two receptors, crosslinking them into a dimeric complex in which the two receptors make no physical contact (**Figure 1**). Receptor-mediated dimerization involves physical contact between receptors with no direct contribution from a ligand (**Figure 2A**). This type of dimerization has been identified in the Epidermal Growth Factor Receptor (EGFR)/ErbB family (Lemmon, 2010). These receptors also display a type of dimerization in which the ligand binds to two different sites within a single receptor instead of crosslinking two receptors, causing a conformational change on the extracellular region (Burgess, 2003). The crystal structure of the extracellular domains of RON suggests that this RTK may form dimers by using both "receptor-mediated" and "ligand-mediated" interactions (**Figure 2B**) (Chao et al., 2012). Furthermore, the orientation of the RON kinase domain upon dimerization is not well defined, but it has been suggested that the C-terminal tail blocks the kinase domain active site during the inactive state as for many other RTKs (**Figure 2B** – green line) (Yokoyama et al., 2005).

In the case of crystalized EGFR kinase domain fragments, these can form an inactive symmetric dimer and an active asymmetric dimer. The asymmetric dimer formed between two kinase domains relies on an activator-receiver model, in which the activator's C-terminal lobe makes physical contact with the adjacent N-terminal lobe of the receiver, causing a conformational change that activates the receiver kinase domain (**Figure 2C**) (Maruyama, 2014). Studies where the activator/receiver

interacting surfaces were mutated in the full-length receptors suggest that the asymmetric dimer formation is important for activation of the full-length receptor (Zhang et al., 2006).

Furthermore, RTK signaling is not only initiated by homodimers, but also by heterodimers within a family such as heterodimerization of EGFR with ErbB2 (Li et al., 2012), or with other families of RTKs. Crosstalk is referred to the influence of one receptor on the signaling activity of a second heterologous receptor and its signaling intermediates. We are interested in the crosstalk of EGFR and RON, two receptors from different families with different apparent mechanisms of activation.

1.2. RTK signaling in cancer research

RTK activity is highly regulated in normal cells, while dysregulation of these receptors has been found in a wide range of cancers. In cancer cells, dysregulated activation of RTKs is caused by gene amplification, mutations, gene re-arrangement, over-expression, or abnormal endocrine, autocrine, or paracrine stimulation of both receptor and ligand (Takeuchi and Ito, 2011). RTKs dysregulation has been correlated with the development and progression of a number of cancers, making them a promising therapeutic target (Takeuchi and Ito, 2011; Prahallad, 2016). Cancer and its connection to aberrant signaling of RTKs has driven the development of drug therapies that inhibit or attenuate RTK activity (Lemmon, 2010).

Resistance to therapies decreases survival rate for cancer patients. Cancer treatment requires new strategies that can provide information behind the complexity of signal transduction pathways and receptor crosstalk (Prahallad, 2016). Structural studies of RTK crosstalk could provide some insight on how aberrant signaling influences the development, progression, and resistance of cancer.

1.3.   EGFR and RON crosstalk

Heterogeneous receptor-receptor interactions play an important role in maintaining cell functions by inducing specific intracellular signaling cascades (Peace, 2003). Two RTKs, RON (Recepteur d'origine nantais) and EGFR are known to co-overexpress on tumors, which results in crosstalk. However, the molecular mechanisms that facilitate this interaction are unknown.

RON is a membrane receptor that binds macrophage-stimulating protein (MSP). The RON receptor is synthesized as a single chain precursor of 185 kDa that is then cleaved into its heterodimeric, mature form before it is trafficked to the cell membrane (Peace, 2003).   The general structure of RON consists of an extracellular ligand-binding domain, followed by a single-pass transmembrane domain and an intracellular beta chain that contains a catalytic tyrosine kinase domain (Peace, 2003). It is known to regulate inflammatory responses in skin, liver, and lung, as well as playing an important role in ovarian development (Peace, 2003). RON is a member of the MET family of RTKs, it is expressed in epithelial tissues, and plays an important role in

cancer (Peace, 2003; Waltz, 1998; Benight and Waltz, 2012; Yokoyama et. al. 2005; Stella et. al. 2018; Faham et. al., 2016; Kang et. al., 2015; Maggiora et. al., 1998). Evidence of overexpression of RON and constitutive phosphorylation of this receptor has been found in a number of epithelial human cancers, such as pancreatic, ovarian, colon, and lung cancer (Maggiora, 1998; Chen, 1997). Cells overexpressing RON have shown an increase in cell proliferation, migration, and branching morphogenesis, all of which may play roles in cancer (Peace, 2003).

EGFR is present in a large number of tissue types, and it contributes to the regulation of apoptosis, proliferation, migration, and differentiation (Sibilia, 1995). EGFR is upregulated in different tumor types due to overexpression or upregulation of signaling mediated by EGFR-ligand stimulation (Peace, 2003). EGFR is a single chain glycoprotein of 180kDa. It consists of a ligand-binding extracellular domain, a single-pass transmembrane domain, and a cytoplasmic kinase domain. EGFR is a member of the erbB family of RTKs and it is known to bind to several ligands, including the epidermal growth factor (EGF) and the transforming growth factor alpha (TGF-α) being the most common and abundant (Peace, 2003; Wells,1999).

Both RON and EGFR are highly expressed in many different tissues They are also associated with cell motility and morphological changes that lead to branching tubulogenesis (Peace, 2003). RON is known to interact with heterologous receptors, and EGFR has been often described as a central player in crosstalk interactions (Peace, 2003, Faham et. al., 2016). Co-immunoprecipitation studies indicate there could be a direct interaction between EGFR and RON similar to other interactions

within the EGFR family and the MET family. This could suggest there is a functional and biochemical interaction between EGFR and RON that plays a role in cellular processes leading to cancer (Ortiz-Zapater et al.,2017; Engelman et al., 2007).

1.4.   Structural studies: Nanodiscs

Studying structural and mechanistic properties of membrane proteins is often difficult. Solubilization is important to maintain target proteins in a stable state that allows for manipulation and analysis. The most common technique to solubilize membrane proteins is through the use of detergents that form detergent-lipid-protein micelles (Mi, 2008). However, the formation of micelles often interferes with a number of assays and optical techniques, and the detergent tends to reduce protein activity as they co-concentrate with the protein, which can lead to denaturation. This often results in the use of protein fragments for structural studies through crystallography that help determine extracellular domain and kinase domain interactions, as it is the case with EGFR, and all four ErbB receptors (Bouyain S, 2005; Cho HS and Leahy DJ, 2002; Cho HS et al., 2003; Ferguson KM et al., 2003; Garrett TP et al., 2003). Many membrane proteins require specific types of lipids to maintain activity, and this characteristic is not well mimicked by detergent micelles. Another approach to study membrane proteins is liposomes that incorporate membrane proteins within the bilayer. In this case, each side of the bilayer is compartmentalized (Sligar, 2016, Mi et al., 2008), and the membrane protein is found in a more native state. However,

liposomes are usually unstable and are difficult to prepare with a controlled size and stoichiometry, generating a homogeneous sample (Sligar, 2016).

Nanodiscs offer a solution to some of these challenges by providing a defined-sized native-like environment to membrane proteins that offers stability to the target protein.

Phospholipid bilayer
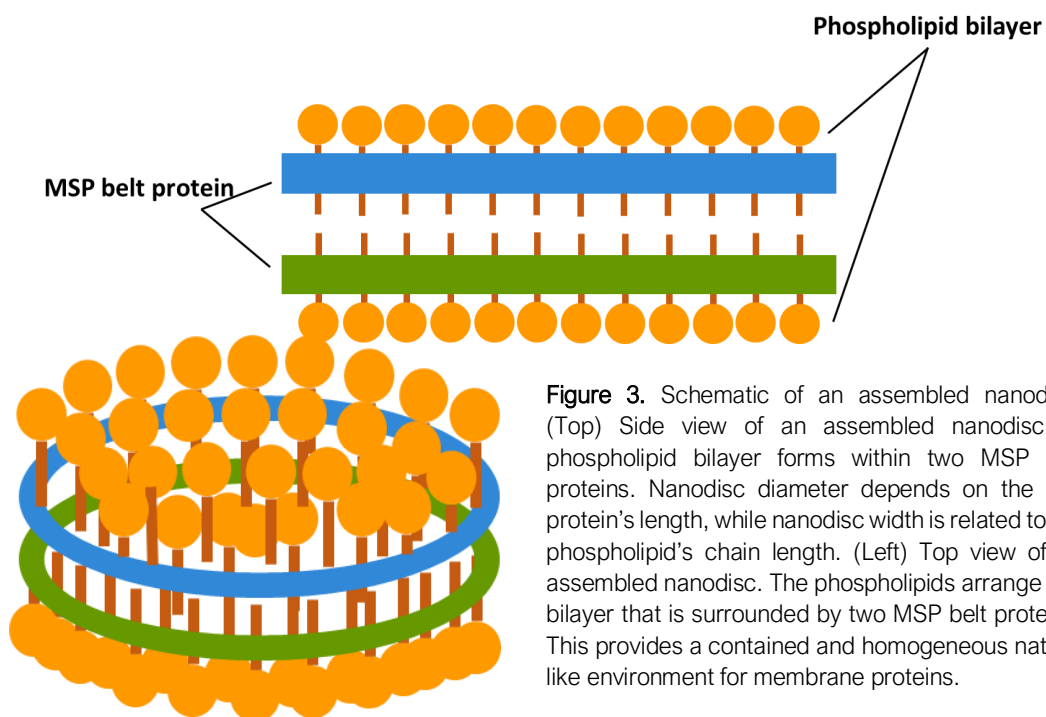
MSP belt protein

Figure 3. Schematic of an assembled nanodisc. (Top) Side view of an assembled nanodisc. A phospholipid bilayer forms within two MSP belt proteins. Nanodisc diameter depends on the belt protein's length, while nanodisc width is related to the phospholipid's chain length. (Left) Top view of an assembled nanodisc. The phospholipids arrange in a bilayer that is surrounded by two MSP belt proteins. This provides a contained and homogeneous native-like environment for membrane proteins.

Important structural information of membrane proteins can be obtained through a variety of biophysical techniques. Critical structural data, such as protein-protein and lipid-protein interactions, as well as detailed images of protein structure, can be facilitated using nanodiscs (Denisov and Sligar, 2013). Nanodiscs provide a native-like environment that increases protein stability and maintains their functionality by preventing aggregation. Given that target proteins remain active and monodisperse in nanodiscs, they are often used in x-ray crystallography, where nanodiscs are used to collect substantial quantities of protein without aggregation (Denisov and Sligar,

2013). Protein embedding into nanodiscs helps with storage and collection of active membrane proteins or receptor fragments for subsequent functional studies.

Nanodiscs have been used for cryo- and negative staining electron microscopy (EM), where the highly homogeneous size of nanodisc preparations help with structural determination. Membrane proteins in nanodiscs are less susceptible to aggregation. This characteristic helps preserve protein function and structure (Denisov and Sligar, 2013). Nanodiscs have been used to decipher the structure of the Tc Toxin, drug efflux pumps, the magnesium channel, the ryanodine receptor, among others (Gatsogiannis et al., 2016; Daury et al., 2016; Matthies et al., 2016; Efremov et al., 2015; Xu et al., 2016; Shenkarev et al., 2018; Gao et al., 2016; Gogol et al., 2012).

Another use is nuclear magnetic resonance (NMR), a technique that is often used to analyze soluble proteins and obtain structural data (Bax, 1989). Protein solution methods usually limit the size of target protein for NMR analysis. Nanodiscs prevent aggregation of membrane proteins and have a defined stoichiometry, making high resolution studies possible (Denisov and Sligar, 2013). NMR techniques, such as solution and solid-state NMR have relied on the use of nanodiscs to provide information on membrane protein structure and function, as well as their interactions with the lipid membrane. Nanodiscs have been used to understand the relationship between the oncogenic protein KRas4b and the lipid bilayer, shedding some light on protein conformational changes linked to protein-lipid interactions (Mazhab-Jafari, 2015; Hagn et al., 2018; Viennet et al., 2019).

Nanodiscs can be fixed to surfaces without losing their structure. This makes them great tools for single molecule studies, such as Atomic Force Microscopy (AFM), single-molecule imaging, and fluorescence spectroscopy (Denisov and Sligar, 2013). Nanodiscs have been used to incorporate K^+ channel protein and study its dynamics using single molecule fluorescence resonance energy transfer (FRET), showing that the presence of PIP_2 causes a conformational change in the channel that is consistent with a "twist-shrink" structural model. In this case, nanodiscs provide a native-like lipid bilayer (Sadler et al., 2016). Single-molecule force spectroscopy has relied on protein incorporation into nanodiscs, including studies on the mechanical unfolding of bacteriorhodopsin (Zocher et al.,2012). Nanodiscs have also been used for single-molecule fluorescence and total internal reflection microscopy to monitor binding of Nile Red and its effects on CYP3A4 embedded into nanodiscs (Nath et al., 2010).

Generally, spectroscopic methods, such as electron spin resonance, optical and electron paramagnetic resonance spectroscopy, and resonance Raman are fundamental to determine membrane protein functionality (Finkenwirth et al., 2015; Luthra et al., 2013; Mak et al., 2015). The use of nanodiscs for these techniques provides a bilayer that allows membrane proteins to maintain their functionality (Denisov and Sligar, 2013). Membrane protein characterization through X-ray and neutron scattering also benefit from the use of nanodiscs. Usually, these techniques are limited by protein size and aggregation, as well as protein orientation, these issues can be solved by using nanodiscs (Denisov and Sligar, 2013). Examples of these include curdlan synthase, cytochrome P450, and the formation of functional trimers

of bacteriorhodopsin (Periasamy et al., 2012; Skar-Gislinge et al., 2015; Bayburt et al., 2006)

Nanodiscs are non-covalent assemblies of phospholipids and a membrane scaffold protein (MSP), a genetically modified apolipoprotein (Borch, 2009; Sligar 2016). The phospholipid acts as a bilayer domain while two MSP molecules wrap around the edges of the discoidal structure in a belt-like configuration, each MSP covering the hydrophobic alkyl chains of each leaflet (**Figure 3**) (Sligar,2016).

The membrane scaffold protein (MSP) is based on the sequence of human apolipoprotein A1 (ApoA-1), which is related to the serum apolipoproteins that are the primary component of high-density lipoproteins (Borch, 2009; Sligar, 2016). MSP is an amphipathic helical belt protein that wraps around a lipid bilayer of defined number of lipid molecules. It is formed by the truncation or repetition of the 11- and 22-residue stretches of the ApoA-1 punctuated by proline and glycine, and its length can be increased by adding additional 22-mer repeat units (Sligar, 2016; Siuda and Tielman, 2015). MSP is often expressed in E. coli from a synthetic gene that can include various affinity tags and different lengths that control overall nanodisc size. In our studies, we use His-tagged MSPs.

The lipid bilayer that forms the nanodisc can be composed of different mixtures of phospholipids and other components, such as cholesterol. The membrane can be tailored in composition to suit the protein of interest or study the effects of the bilayer environment on the function of the membrane protein.

Nanodisc size is strictly related to MSP length, area per phospholipid, and number of phospholipids. This means that a defined phospholipid to MSP ratio during assembly leads to homogeneous nanodisc size (Borch, 2009). If the lipid ratio is too high, populations of large MSP-lipid aggregates will form along with the nanodiscs, this is due to the fact that a higher area to perimeter is needed to match the length of hydrophobic MSP belt to the amount of total phospholipid (Sligar, 2016; Bayburt TH, Grinkova YV, Sligar SG, 2002). If lipid to MSP ratio is too low, conditions are unfavorable for disc formation and MSP will form MSP-rich aggregates or nanodiscs that are prone to deformation (Sligar, 2016; Bayburt TH, Grinkova YV, Sligar SG, 2002)

To form nanodiscs, first detergent, phospholipid micelles and MSP are mixed together. Self-assembly of nanodiscs is then triggered by detergent removal. Detergent can be removed through adsorption treatment using porous polystyrene beads or through dialysis. Nanodiscs form most efficiently near the phospholipid phase transition temperature, because of the effects of phase behavior on size and organization of the phospholipid/detergent micelles (Borch, 2009; Sligar, 2016). To incorporate a membrane protein of interest into nanodiscs, the purified protein is usually pre-solubilized with a compatible detergent such as DDM and is mixed with the nanodisc components prior to detergent removal. Once the detergent is removed, membrane protein-lipid and lipid-lipid interactions occur as the bilayer is formed incorporating the protein within the nanodisc and keeping it in a native-like configuration (Borch, 2009; Sligar, 2016).

Specific Aims

Protein structural studies provide mechanistic insight into receptor conformational changes and interaction interfaces that initiate important signaling pathways. These pathways are triggered by proteins whose mechanisms of dimerization and structure-function are not entirely defined. The structure of the epidermal growth factor receptor (EGFR), its activation by ligand, and subsequent homodimerization have been well studied by our group and others. However, recent evidence of crosstalk between EGFR and other receptors, such as the Met receptor family, has led us to explore how these different receptors might interact. Aberrant activation of RON and EGFR due to crosstalk, can lead to tumorigenesis. Although these receptors can be co-immunoprecipitated, the structural requirements for their interactions are not known. Throughout this work we focus on developing a nanodisc assembly protocol that allows us to incorporate full-length RON or EGFR receptors into nanodiscs, ultimately to facilitate studies of RON and EGFR dimerization. To achieve this, this work has two specific aims:

Aim 1: Optimize a nanodisc assembly and protein incorporation method for full-length transmembrane proteins

Membrane protein structural studies are often difficult due to the lack of a proper environment for protein solubilization and receptor size. The general structure of EGFR has been determined by crystallization using individual domains of the receptor. Structural and function studies on membrane proteins often use micelles to

incorporate these proteins, but these are oftentimes large and unstable. Nanodiscs provide a membrane-like environment that allows for solubilization of proteins in a native setting of homogeneous size that maintains the receptor's conformation and functionality. Nanodiscs have been used previously to solubilize many proteins, such as Rhodospin, Neurokinin 1 Receptor (NK1R), Integrin-linked kinase (ILK), including EGFR (Bayburt et. al., 2007; Gao et. al., 2012; Dobreva et. al., 2008; Mi et. al., 2008). We rationalized that by optimizing the nanodisc size and lipid content, we could optimize the incorporation of proteins into the nanodisc. This is especially important in the case of receptor dimers that require a larger lipid surface. Considering this, we tested two belt-proteins that form nanodiscs of two different sizes, and we tested multiple phospholipids of different chain lengths to see if these influence protein incorporation.

Aim 2: Determine a method to best detect protein incorporation into nanodiscs

Identifying protein incorporation into nanodiscs is often achieved through size-exclusion chromatography or native gel electrophoresis. In this work, we had the goal of finding a reliable method to detect receptor incorporation in nanodiscs, particularly in small preparations. We have compared the use of size-exclusion chromatography, gel electrophoresis, affinity purification of proteins, and advanced microscopy techniques to detect protein incorporation.

CHAPTER 2: METHODS

HEK293 Protein production

HEK293 adherent cells were transfected with recombinant proteins, Full-length RON-mNG-SBP (mNeonGreen-Streptavidin Binding Peptide) and Full-length EGFR-SBP (Streptavidin Binding Peptide) and established. Cells were cultured for at least two passages to allow recovery from thaw, and G418 was used as selective agent after thaw. Initially, cells were cultured in a T75 and exponentially subcultured into 6-8 T175 before harvest.

Cycloheximide Treatment

HEK293 cells transfected with full-length RON were treated with a 50 mg/mL solution of Cycloheximide in DMSO for 4 hours at 37 °C before harvest. Cells were harvested once reaching 95% confluency using a cell scrapper and were lysed (20 mM Tris pH 8.0, 400 mM NaCl, 10% glycerol, 0.2% DDM, 1 mM EDTA).

Transient transfection of recombinant proteins in Expi293F cells

Expi293F cells (Gibco A14635) are grown as suspension cultures in a 37°C incubator at 8% CO2 with shaking at 125 rpm. Cells were thawed and grown for at least two passages to allow them to recover. Cells were prepared for transfection by seeding them at a density of $3x10^6$ cells/mL in a 30 mL culture. These cells were then

transfected as per the manufacturers protocol by mixing 30 µg of plasmid with ExpiFectamine 293 reagent (Gibco) to form lipid-DNA complexes. Expifectamine Enhancer Reagents 1 and 2 were added 24 hours after transfection. The transfected cells were incubated for an additional 2 days before harvest.

Test for protein expression

A 500 µL aliquot of the transfected cells was fixed and labeled with fluorescent antibodies for confocal imaging to observe protein expression and localization. Half of the aliquoted cells were fixed in 2% PFA-PBS for 20 min at room temperature, while the remaining half were permeabilized in 0.05% Triton X-100/Hoechst. Cells were labeled with primary antibodies to label RON (RON β-E3 (sc-74588), Santa Cruz) or EGFR (EGFR XP, Cell Signaling D38B1) or with fluorescently labeled ligand, EGF-A488. Labeling agents were added directly to the media and incubated for 1 hr in at a dilution of 1:100 dilution in 3% BSA-TBS. Cells were incubated with secondary antibodies diluted at 1:200 in 3% BSA-TBS. Cells were washed with PBS and centrifuged to recover the pellet. 2µL of the cell pellet were mounted on a slide with Prolong Gold and cured overnight at room temperature.

Protein purification

Transfected cells were lysed (20 mM Tris pH 8.0, 400 mM NaCl, 10% glycerol, 0.2% DDM, 1 mM EDTA) and left on ice for 1 hour with vortexing every 5 min. The lysate

went through three freeze-thaw cycles at -80 ˚C, then was ultracentrifuged and the cell debris pellet was discarded.

Protein was purified using the InterPlay Mammalian TAP system from Agilent (240104) that uses Streptavidin resin to bind SBP-tagged proteins. The streptavidin resin (Agilent - 240105) was washed 3 times using Streptavidin Binding Buffer containing 20 mM Tris pH 8.0, 400 mM NaCl, 10% glycerol, 0.1% DDM, 1 mM EDTA, and 10 mM 2-Mercaptoethanol. The lysate was then separated into individual 1 mL aliquots, and 100 μL of washed resin was added. The mixture was incubated overnight at 4° C with gentle shaking. After centrifugation and removal of the supernatant, each aliquot was washed with Streptavidin Binding Buffer (20 mM Tris pH 8.0, 400 mM NaCl, 10% glycerol, 0.1% DDM, 1 mM EDTA, 10 mM 2-Mercaptoethanol). Samples were incubated for 2 hrs. in Streptavidin Elution Buffer (0.2% Biotin, 20 mM Tris pH 8.0, 400 mM NaCl, 10% glycerol, 0.1% DDM, 1 mM EDTA, and 8.6 mM 2-Mercaptoethanol) to elute the SBP-tagged proteins through affinity competition with Biotin. The eluate was recovered and stored at -80 ˚C.

Protein dialysis and Protein concentration assays

The recovered eluate (1 mL) was dialyzed to remove any traces of Biotin by using a dialysis cassette of 10K MWCO and 4 L of TS Buffer (50 mM Tris/HCl pH 8.0, 150 mM NaCl, and 0.05% DDM). The cassette was suspended in the exchange buffer and incubated for 4 hours at 4 ˚C with low stirring. A Bicinchoninic acid assay (BCA) was performed to measure the concentration of the purified protein using a BCA

protein assay kit (Pierce, 23227) and a plate reader set to measure absorbance at 562 nm. Albumin Standards (BSA) were used to build the standard curve and calculate protein concentration of the dialyzed eluate. Because excess biotin in the elution buffer can affect BCA assay results, an additional method was used to measure protein concentration. The dialyzed eluate and a series of BSA standards were analyzed by SDS-PAGE. The gel was stained with Coomassie blue for 1 hour and de-stained for 2 hours before imaging. Protein concentration was estimated through volumetric analysis of the Coomassie bands and linear regression was used to build a standard curve with the BSA standard bands.

Nanodisc assembly

For nanodisc assembly, three types of zwitterionic lipids were tested, 1,2-dimyristoyl-sn-glycero-3-phosphocholine (DMPC), 1-palmitoyl-2-oleoyl-glycero-3-phosphocholine (POPC), and L-α-phosphatidylcholine (Egg PC). All of these were purchased from Avanti Polar Lipids in chloroform solution. A specific volume of lipids according to sample number and lipid fraction per sample was added to 13 x 100 mm borosilicate glass test tubes and dried with Nitrogen gas. The tube was then placed in a desiccator overnight to allow evaporation of chloroform traces. The lipids were then hydrated in 10 mM Tris pH 8.0, 100 mM NaCl, 10% glycerol, and 20 mM DDM to a final concentration of 10 mM and transferred to a 1.5 mL tube. The mixture was sonicated in a water bath using 1 min pulses. The solution was then left on ice for 30 – 40 min until it appeared clear. Two types of membrane scaffold proteins were used,

MSP1D1 (9 nm final nanodisc diameter) and MSP1E3D1 (12 nm final nanodisc diameter). Both were purchased from Cube Biotech (MSP1D1- 26122, MSP1E3D1 – 26152). The membrane scaffold proteins were reconstructed by resuspending them in ultrapure water and 5% glycerol to avoid aggregation.

A range of MSP:lipid ratio was tested for nanodisc assembly as described in the Results. Ultimately, a 2:150-200 MSP:Lipid ratio was selected as optimal. We attempted to have as close to 6 µM of purified full-length EGFR as possible for each preparation. Phospholipid nanodiscs were assembled in the absence or presence of EGFR. Nanodiscs containing EGFR dimers were assembled with EGFR pretreated with EGF for 10 min at a 1:2 EGFR:EGF ratio prior to adding any other components. The final volume of each sample was 300 µL. All samples were incubated on ice for 1 hour before detergent removal. After this period, BioBeads were used to induce nanodisc assembly through detergent removal. Nanodiscs were incubated overnight at 4 ˚C with gentle agitation. The samples were spun-down to collect the supernatant containing the assembled nanodiscs and the BioBeads were discarded. Ultracentrifugation was then carried on at 50k rpm for 20 min to remove any aggregates. The supernatant was recovered, each sample was aliquoted and stored at -80 ˚C.

Native-PAGE analysis

Loaded nanodisc samples were loaded on a Native-PAGE to search for band colocalization between target protein and MSP belt protein. 25 uL of nanodisc sample were mixed with 2x native buffer (Bio-Rad 1610738) before loading in a 4-15% precast gel (Bio-Rad 456-1084). Gel was run at 125 V for 1 hr at room temperature and was transferred onto a nitrocellulose membrane. The membrane was blocked with 3% BSA-TBS for 40 min and incubated overnight with primary antibodies (RON β-E3 – Santa Cruz sc-74588; EGFR XP – Cell Signaling Technologies 4267L; His-tag XP – Cell Signaling Technologies 12698S). Secondary fluorescent antibodies were added and incubated for 1 hr at room temperature. The membrane was rinsed and imaged on the Li-Cor Odyssey Fc (Li-Cor – 2800).

Size exclusion chromatography

Size exclusion chromatography of assembled samples was performed to separate EGFR-loaded nanodics from empty nanodiscs using a GE Superdex 200 Increase 30/100 column (GE - 28990944). Molecular weight standards ranging from 29 kDa to 700 kDa (Sigma-Aldrich - MWGF1000-1KT) were run prior to each batch of samples. 100 μL per sample were run separately using 1.5 column volumes (CV) or 36 mL of TSG10 buffer (50 mM Tris/HCl pH 7.9, 100 mM NaCl, 10% glycerol) per run and keeping the pressure in the column below 3 MPa. The column was washed with

2 CV of TSG10 in between each sample. Fractions of about 0.5 - 1 mL were collected for each peak for further analysis.

His-Tag Pull-down

Nanodiscs were purified by His-tag affinity with Ni-NTA coated agarose beads using the ProBond Purification Systems (Invitrogen - K85001) under Native conditions, using the 5x Native Purification Buffer (250 mM NaH_2PO_4 pH 8.0, 2.5 M NaCl). As controls, MSP1E3D1 alone and free EGFR were used, as well as empty nanodiscs.

ProBond slurry was resuspended and washed with ultrapure water and native binding buffer (NBB - 50 mM NaH_2PO_4 pH 8.0, 0.5 M NaCl) before usage. 200 µL of each nanodisc sample were used and NBB was added for a final volume of 300 µL per sample. Each sample was added to 50 µL of ProBond slurry and left on rotation for 1 hr at 4 °C. The samples were spun down at low speed for 1 min, and the supernatant was collected for SDS-page analysis. The resin was washed 4 times with 200 µL of Native Wash Buffer (50 mM NaH_2PO_4 pH 8.0, 0.5 M NaCl, 20mM imidazole). Samples were spun down at low speed between every wash and the supernatant was kept for further analysis. The Ni-NTA agarose beads were denatured using 20 µL of 2x Laemli reducing buffer and were boiled for 5 min.

An SDS-page was loaded with 20 µL of each sample's denatured agarose beads, along with supernatant and wash 1 and 4 per sample, including controls. SDS-page was run for about 1 hr at 125 V. The gel was transferred to a nitrocellulose membrane

and stained using REVERT total protein stain (Li-Cor - 926-11021) for 5 min. The membrane was rinsed twice for 30 seconds using REVERT wash solution (Li-Cor - 926-11022), and then washed 3 times using ultrapure water. The membrane was then imaged on the Li-Cor Odyssey Fc (Li-Cor – 2800).

EGFR Immunoprecipitation

40 µL of empty nanodisc sample and purified EGFR as well as 20 µL of MSP1E3D1 were diluted separately in 300 µL of TSG10 to be used as controls for EGFR immunoprecipitation. 10 µL of EGFR (clone R-1) conjugated agarose resin (Santa Cruz - sc101 AC) were used for immunoprecipitation of each sample. Samples and resin were added to separate 1.5 mL tubes. Samples were incubated overnight at 4 °C on rotation. Samples were spun down at 2000 xg for 5 minutes at room temperature to remove the supernatant. Supernatant was stored for further SDS-PAGE analysis. The resin was washed 8 times with 300 µL of TSG10. To denature the resin, 25 µL of 2x Laemli reducing buffer were added and boiled for 5 minutes. 40 µL of the supernatant were denatured using 6x Laemli reducing buffer and boiled for 5 min. Samples were loaded on an SDS-PAGE. SDS-page was run for about 1 hr at 125 V. The gel was transferred to a nitrocellulose membrane and stained using REVERT total protein stain (Li-Cor - 926-11021) for 5 min. The membrane was rinsed twice for 30 seconds using REVERT wash solution (Li-Cor - 926-11022), and then

washed 3 times using ultrapure water. The membrane was imaged on the Li-Cor Odyssey Fc (Li-Cor – 2800).

Transmission Electron Microscopy imaging of EGFR and nanodiscs

Purified EGFR or EGF-treated EGFR were diluted 1:100 in PBS and stored on ice. Purified empty or loaded nanodiscs were diluted 1:10 in PBS and stored on ice. Carbon film (3-4 nm) 200 mesh nickel finder grids (Electron Microscopy Sciences - EMS200-Ni) were glow discharged, and 5ul of sample were adsorbed to grids for 3 minutes. Grids were floated on water droplets twice for ten seconds, and then stained twice with 0.75% uranyl formate (Electron Microscopy Sciences - 22400) for 10 seconds. The grids were wick dried with filter paper prior to storage. EGFR and EGFR-loaded nanodiscs were labeled with colloidal gold, nanodiscs were adsorbed to flow discharged grids, washed with PBS, and fixed for 5 minutes with 1% paraformaldehyde (Electron Microscopy Sciences - 15700). The grids were floated on 50mM glycine/PBS for 5 minutes and blocked with 0.1% BSA/PBS for 5 minutes. Streptavidin or anti-his Nanogold (10 nm) was diluted 1:100 in 0.1% BSA/PBS and samples were labeled for 15 minutes. Grids were floated on water droplets three times for ten seconds and twice on droplets of 0.75% uranyl formate for ten seconds. The grids were wick dried with filter paper prior to storage.

Images were acquired on a Hitachi 7700 Transmission Electron Microscope at a magnification range of 50,000X-100,000X and drift correction.

Single Nanodisc Imaging

Coverslip preparation. 25 mm coverslips were Piranha treated prior to their use to remove organic residues from the glass surface. Coverslips were allowed to dry before drawing 2 x 2 array on each one using a hydrophobic PAP pen. Once the array was drawn, the coverslips were dried and placed in a humidified container. Biotin-PEG and mPEG were diluted in 10mM solution of sodium bicarbonate buffer pH 8.5 at 6.4 mg/mL and 250 mg/mL, respectively. The solution was spun down at 10,000 xg for 1 min at room temperature to remove bubbles. The solution was applied to each array and all coverslips were left incubating in a humidified container for 3 to 4 hrs at room temperature while protected from the light. Coverslips were washed repeatedly with ultrapure water and dried with nitrogen. Coverslips were stored at -20 °C in a sealed parafilm-lined container and were used within a week.

Coverslip surface functionalization. Surfaces were functionalized in a manner similar to that described in Salazar-Cavazos et. al., 2018. Arrays on 25 mm coverslips were equilibrated to room temperature and placed on a TC100 plate lined with parafilm. Each region of the array was treated with a 10 mg/mL $NaBH_4$/PBS solution for 4 min at room temperature and washed 3 times with PBS. Each array was treated with 0.2 mg/mL of NeutrAvidin (Thermo Scientific – 31000) in T50 Buffer (10 mM Tris pH 8.0, 50 mM NaCl). Then, each region was treated with either biotinyated α-EGFR (Leinco - E101) or biotinylated α-His Tag (Thermo Fisher Scientific MA1-21315-BTIN) for 10

min at room temperature. Each coverslip was washed 3 times with T50-BSA (10 mM Tris pH 8.0, 50 mM NaCl, 0.1 mg/mL BSA). EGFR-embedded nanodisc samples were diluted 1:250 in PBS. Free EGFR (1:1000 in PBS) and empty nanodiscs (1:250) were used as controls. All arrays were placed on ice, samples were then added to their respective area on the array and left incubating for 10 min. The arrays were washed 4 times with T50-BSA.

Nanodisc Labelling. DiD (ThermoFisher Scientific - V22887) was used to label the nanodiscs and was diluted 1:2000 in T50-BSA, along with α-EGFR AF555 conjugate (Cell Signaling – 5108) at a 1:50 dilution to label EGFR. The lipid dye and the fluorescent antibody were added to the array and incubated for 1 hr on ice. The array was then washed 6 times with T50-BSA and then twice with cold PBS before imaging.

A second set of coverslips with 2x2 arrays were treated with Neutravidin only. Loaded nanodiscs were pulled down by using affinity precipitation between Avidin and SBP-tagged EGFR. Nanodisc samples were incubated on Neutravidin-treated coverslips for 10 min. The arrays were washed with T50-BSA 4 times and labelled with α-EGFR R-1 clone AF647 (Santa Cruz - sc101) and α-His XP AF488 (Cell Signaling Technology - 14930S) conjugates at a 1:50 dilution to label EGFR and His-tagged MSP1E3D1, respectively. Each area of the array was washed again as described above.

Single Nanodisc Imaging. The array was equilibrated to room temperature for 5 min prior to imaging. Each area on the 2x2 array on the 25 mm coverslip was imaged on a custom-built system from an inverted microscope (IX71, Olympus America Inc) (Schwartz et al., 2017; Valley et al., 2015). 642 and 561 lasers were used at a laser power of 5 mW and 1 mW, respectively. These lasers were coupled into a multi-mode fiber (P1-488PM-FC-2, Thorlabs) and focused onto the back focal plane of the objective lens with a 1.45 NA (UAPON 150XOTIRF, Olympus America Inc.) (Schwartz et al., 2017; Valley et al., 2015). Sample illumination and emission were achieved using a quad-band dichroic and emission filter set (LF405/488/561/635-A; Semrock). A band-pass filter (685/45, Brightline) was used for emission light filtering. Emission was collected on an electron-multiplying charge-coupled device (EM CCD) camera (iXon 897 – Andor Technologies. Images were 256 x 256 pixels per channel, with each pixel being 0.1067 µm. The emission path includes a quad band optical filter (Photometrics, QV2-SQ) with 4 filter sets (600/37, 525/45, 685/40, 445/45, Brightline) and the EM CCD camera mentioned above (Schwartz et al., 2017; Valley et al., 2015).

CHAPTER 3: RESULTS

3.1. Protein purification and nanodisc assembly

3.1.1. Protein purification method

The first step required for structural studies of EGFR and RON interactions was to produce and purify receptors. To maintain receptor functionality and insure proper expression and conformation, full-length EGFR and RON plasmids were transfected into the human embryonic kidney cell line, HEK293. Stable cell lines expressing EGFR or RON were selected using G418. For purification, both plasmids expressed a Streptavidin-Binding Peptide tag (SBP-tag) at the C-terminus of the receptor. The SBP-tag is a 38-amino acid sequence that can bind to streptavidin but has a lower affinity for streptavidin than biotin's affinity for streptavidin. SBP-tagged proteins can be purified using streptavidin agarose resin and eluted from the beads by adding biotin. This purification method has been used previously to purify EGFR protein for nanodisc assembly (Mi et al., 2008). Streptavidin purification is ideal for structural studies on full-length receptors as it preserves protein functionality and structure by using gentle elution conditions, and thus avoiding protease digestion. The streptavidin protocol also uses freeze-thaw cycles for cell lysis. Freeze-thawing is a cell disruption
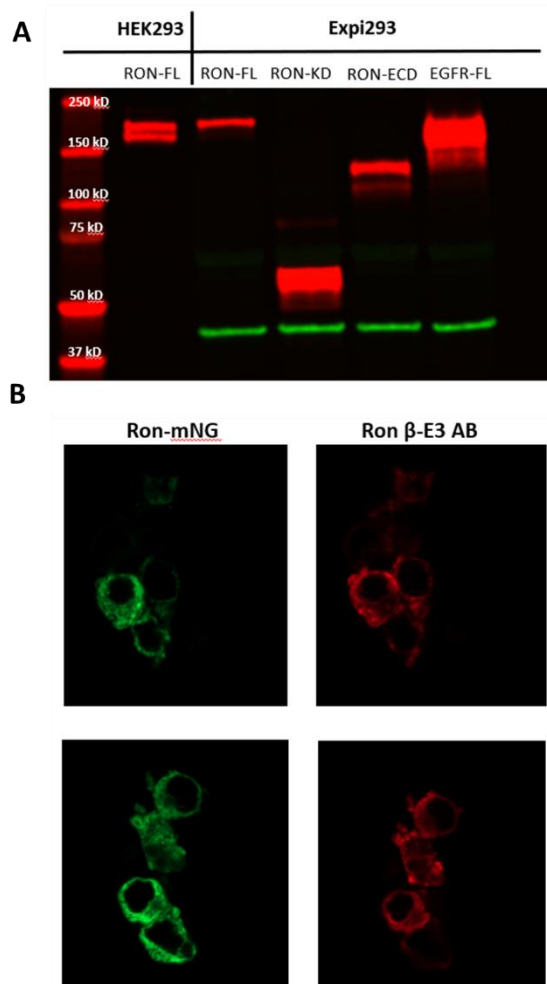
Figure 4. A. Transient transfection of recombinant protein in Expi293F cells. Purified protein from Expi293F cells transiently transfected with full-length RON, RON fragments (Kinase domain (KD), and Extracellular domain (ECD)), and full-length EGFR. Lane 1 shows purified full-length (FL) RON from HEK293 cells after CHX treatment, while lane 2 shows the same recombinant protein in Expi293F cells. The top band (white arrow) indicates pro-RON. B. Confocal imaging of Expi293F cells transfected with RON FL show unprocessed RON sequestered in the Endoplasmic Reticulum instead of localized on the cell membrane. RON detected using the mNeonGreen tag (mNG) (green), and the RON β E3 antibody (red)

method that allows lysis of the cells without sonication or the addition of harsh detergents, which could denature the proteins.

Purification from HEK293 adherent cells resulted in low protein yield that was not optimal for nanodisc incorporation. Previous work suggested 26.5 µg of target protein was needed for each nanodisc preparation (Mi et al., 2008). About six T175 flasks totaling in 6×10^8 HEK293 cells yielded about 6 µg of target protein after elution. This eluate with a concentration of 30 µg/µL needed to be concentrated using centrifugal concentrators, which caused protein losses due to non-specific binding to the concentrator's membrane. After concentration, the entire eluate was used for a single nanodisc preparation, making it difficult to run any additional controls. Therefore, a modified high-density suspension cell line (Expi293F, Gibco), a derivative of HEK293,

was transiently transfected with full-length RON, RON Kinase domain (RON-KD), RON extracellular domain (RON-ECD), as well as full-length EGFR. **Figure 4A** shows the total lysates of full-length receptors and protein fragments. The Expi293F cell line has been optimized for high protein production. With this system, we obtained a higher yield of around 0.25 – 0.3 mg, while still culturing in human cells. Initially, this cell line was not fully processing the full-length RON receptor. This can be observed in the blot (**Figure 4A**), and in confocal imaging of the cells where RON appears to be in the Endoplasmic Reticulum rather than localizing to the plasma membrane (**Figure 4B**).
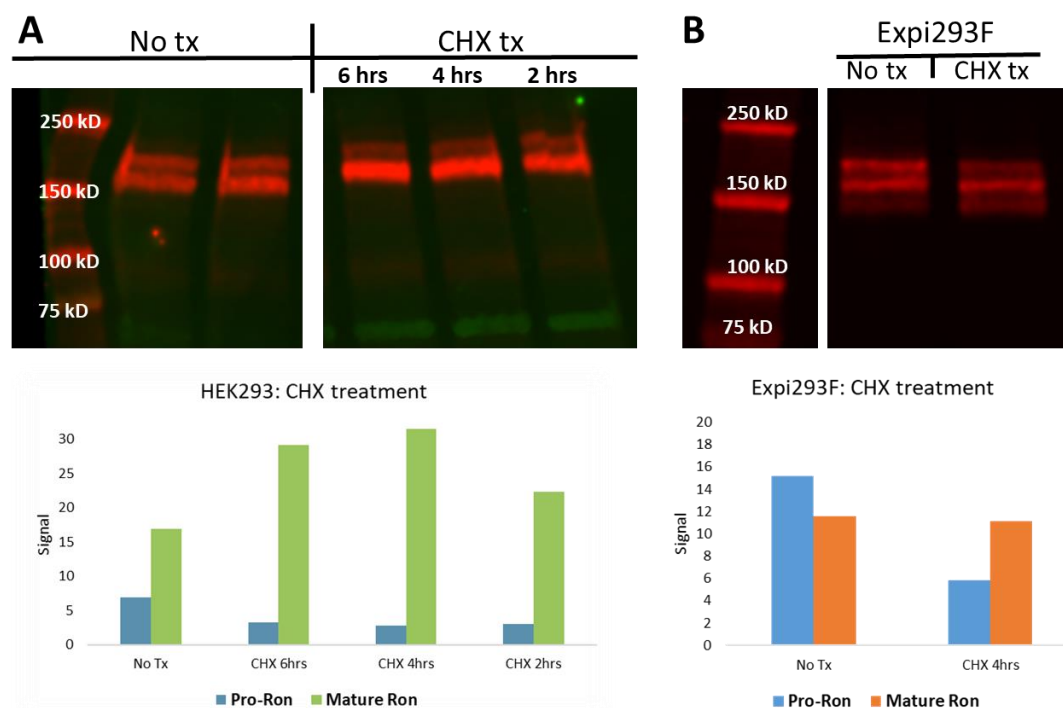
Figure 5. **A.** CHX treatment on HEK293 and Expi293F cells for RON processing. Total lysate of HEK293 adherent cells with no treatment, and after 2, 4, and 6 hrs of CHX treatment. Untreated cells have a high content of pro-RON (top band), while treated cells have a larger ratio of mature RON (lower band). The graph bellow shows that CHX treatment reduces the Pro-RON to RON ratio from 1:2 to approximately 1:10. **B.** CHX treatment on Expi293F cells expressing RON FL. Untreated cells have an almost 1:1 ratio of pro-RON (top band) to RON (bottom band). After a 4 hr CHX treatment, total lysate shows a decrease on pro-RON to a 1:4 ratio.

The RON gene encodes a 190 kDa protein (pro-RON) that is intracellularly cleaved and re-arranged into a two-chain heterodimeric receptor with a 40 kDa α-chain, and a 150 kDa β-chain held together by disulfide bonds (Peace, 2003). These two forms can be distinguished on the western blot in **Figure 4A, lane 1,** which corresponds to a purified sample of RON expressed in HEK293 cells. The α-chain is entirely extracellular, while the β-chain comprises an extracellular domain, a single-pass transmembrane domain, and a larger cytoplasmic domain where the tyrosine kinase resides. For RON cleavage and re-arrangement to occur, the single chain Pro-RON undergoes proteolytic cleavage at a specific site (K^{305} – R – R – R – R^{309}) that breaks the peptide bonds between amino acids and generates mature RON. Without this conversion, RON cannot be activated.

Given this characteristic processing of RON, cells transfected with full length RON plasmid were cultured and treated with Cycloheximide (CHX), a protein synthesis inhibitor that prevents translational elongation, thus inhibiting pro-RON production. The majority of RON receptors will mature during the incubation with CHX, increasing the ratio of processed to pro-RON forms in the preparation (**Figure 5A**). After CHX treatment, total lysates were analyzed by western blotting for the SBP-tag. HEK293 cells treated with CHX saw a reduction in the Pro-RON to RON ratio from 1:2 without treatment to 1:10 with treatment according to blot quantification (**Figure 5A, graph**). After optimization of growth conditions, CHX treatment was also tested on the Expi293F cells. The total lysate after treatment was analyzed by western blotting for

the SBP-tag (**Figure 5B**). CHX treatment for four hours also increased the fraction of mature RON in the Expi293F cells from a 1:1 to 1:4 pro-RON:RON ratio.

For purification of full-length receptors from the Expi293 lysates, we followed the general protocol for purification of SBP-tag proteins and optimized it to better fit our system.

For efficient binding and elution, we found that dividing the total lysate into 5 to 6 1 mL batches and adding 100 µL of streptavidin resin increased purification efficiency. This small batch processing decreased protein losses. Large batch processing may be less efficient due to improper contact of the resin with the elution buffer or resin drying out in the larger 15 mL tubes. To increase protein elution, we doubled the concentration of biotin present in the elution buffer

Figure 6. Streptavidin affinity-based purification in small-batch mode shows the amount of protein in each sample in relation to the total protein in the initial lysate. The supernatant (2nd lane) shows a very small amount of EGFR unbound to the resin. The first elution (3rd lane) shows a protein rich sample, while the second elution (4th lane) indicates that nearly all protein is eluted in the first elution. 1-2% protein remains stuck to the resin (5th lane) despite the two elutions. Protein recovery is shown in the graph bellow

by using 0.2% biotin instead of the suggested 0.1%. This increase in biotin concentration should not have adverse effects on protein functionality or structure. The purification process of EGFR using the small-batch process is shown on the blot

in **Figure 6**. Binding of the receptor to the beads is seen as a decrease in receptor levels in the supernatant. Purified protein in the eluate is shown on the right. Unbound protein remaining in the supernatant and residual protein bound to the resin was quantified based on the volume of the eluate to determine protein losses during the purification process. Approximately 9-10% of the protein did not bind to the resin and was lost in the supernatant, while 1-2% of target protein was lost by remaining bound to the streptavidin resin **(Figure 6)**.

The purification process was initially tested using two detergents, n-dodecyl-β-D-maltoside (DDM) and Triton X-100. No difference in the purification process was observed between the two detergents. No difference in the purification process was observed between the two detergents. Therefore, given EGFR's solubility in DDM and the detergent's ability to preserve the receptor's functionality (Mi et al., 2008), DDM was used rather than Triton X-100 or the standard NP40.

We found that the biotin in the elution buffer affects protein quantification by standard BCA methods. Even a 1:100 dilution of the biotin buffer alone caused a rapid color change in the BCA assay. Concentration and buffer exchange of the eluate to remove excess biotin was attempted using centrifugal concentrators with a low molecular weight cut-off (MWCO). This resulted in protein losses due to non-specific binding to the concentrator's membrane. Therefore, we developed an alternative quantification method where the protein concentration of the eluate was estimated using BSA standards on an SDS-PAGE gel. The gel was stained with Coomassie Blue, and the
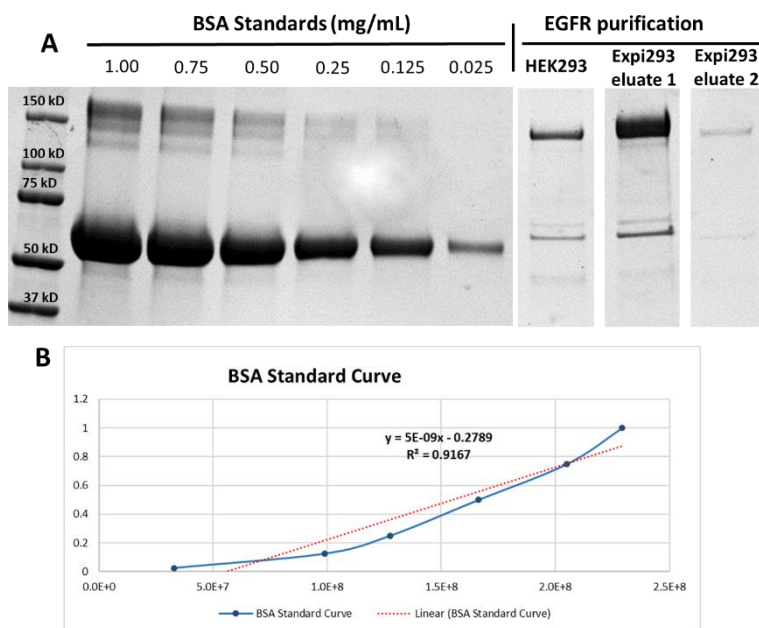
Figure 7. A. BSA standard SDS-PAGE for protein quantification. BSA standards were run in an SDS-PAGE along with full-length EGFR purified from HEK293 cells and Expi293F cells. The gel was stained with Coomassie Blue. B. A standard curve was built using these standards to calculate the concentration of purified EGFR.

BSA bands were quantified to create a standard curve. The concentration of purified EGFR and RON receptors was then estimated using the BSA standard curve as shown in **Figure 7.** We obtained around 200– 300 µg of target protein from Expi293F cells (**Figure 7, lane 8** – Expi293F Eluate 1). As mentioned above, HEK293 cells yielded approximately 20-25 µg during the first elution, needing further concentration for nanodisc assembly (**Figure 7, lane 7**– HEK293 eluate 1). Based on previous work (Mi, et al., 2008) we used 75 µL of the first elution from Expi293F cells for a final concentration of 1 µM or 13.5 µg of EGFR as suggested.

3.1.2. EGFR dimers and RON incorporation in nanodiscs

Previous work in our group tried to incorporate EGFR and RON into pre-formed nanodiscs (Cube Biotech). Although this worked for receptor fragments, the full-length receptors were never incorporated based on native gels. We concluded that

the bulky domains on either side of the transmembrane domain of these receptors likely prevents them from spontaneously incorporating into pre-formed nanodiscs. The alternative method is to assemble nanodiscs from their components around the protein to be embedded. For assembly, we started with purified protein in detergent micelles combined with MSP belt protein and phospholipids. Nanodisc assembly is initiated by removing the detergent. The ratio of belt protein, lipids, and receptor is critical for proper nanodisc formation. Here we optimized nanodisc assembly by testing ratios of MSP:Lipid:membrane protein, as well as testing two sizes of nanodisc and different phospholipids. Different belt proteins can form nanodiscs with specific diameters, and the choice of nanodisc size should be based on the size of the embedded protein of interest. EGFR is a membrane protein with an extracellular domain and a cytoplasmic kinase domain, both of which are of considerable size. These two domains are linked by a single-pass transmembrane domain that, upon nanodisc assembly will be embedded within the lipid membrane of the nanodisc. Taking these structural characteristics of our target protein into account, nanodiscs were assembled using two Membrane Scaffold Proteins (MSPs) that produce nanodiscs of two different diameters. Phospholipids with different carbon-chain length were also tested to achieve proper embedding of the transmembrane domain based on nanodisc thickness. Target proteins (Full-length EGFR or RON) were added to the nanodisc mixture simultaneously with the MSP belt protein and hydrated phospholipids. Detergent was removed using non-polar polystyrene adsorbent beads.

3.1.3. MSP1D1 and DMPC nanodiscs

Our first experiments were based on previous literature of EGFR incorporation in nanodiscs (Mi et al., 2008). We used a mixture of the standard-sized belt protein MSP1D1 and DMPC at a 2:100 ratio. DMPC is a saturated 14-carbon chain synthetic phospholipid that is regularly used in liposomes and lipid bilayers. MSP1D1 is a belt protein that yields nanodiscs of 9.6 nm in diameter. To detect incorporation of full-length receptor into the nanodiscs, we analyzed the nanodisc samples by native-PAGE. Nanodisc preparations were loaded and run on a native-PAGE without denaturing. The native gel was stained with Coomassie blue or transferred onto a nitrocellulose membrane and labelled with primary antibodies against His-tag to detect MSP1D1, and against RON or EGFR to detect the receptor. Fluorescent secondary antibodies were used to detect both MSP1D1 and the receptor labeling on the same gel. The native-PAGE separates the nanodiscs from the unincorporated target proteins and the protein-loaded nanodiscs from the empty based on their mass to charge ratio. If the receptor was incorporated into nanodiscs, we expected to see colocalization of MSP1D1 and the target protein (EGFR or RON) in a higher molecular weight band (**Figure 8A**). Empty nanodiscs were run as a control. Based on these experiments, we found colocalization between a higher nanodisc band and the band representing the target protein, indicating potentially loaded nanodiscs. **Figure 8A** shows colocalization of the EGFR and nanodisc band (yellow) which suggests EGFR-loaded nanodiscs. However, the incorporation is not efficient when compared to the empty nanodisc band (green).

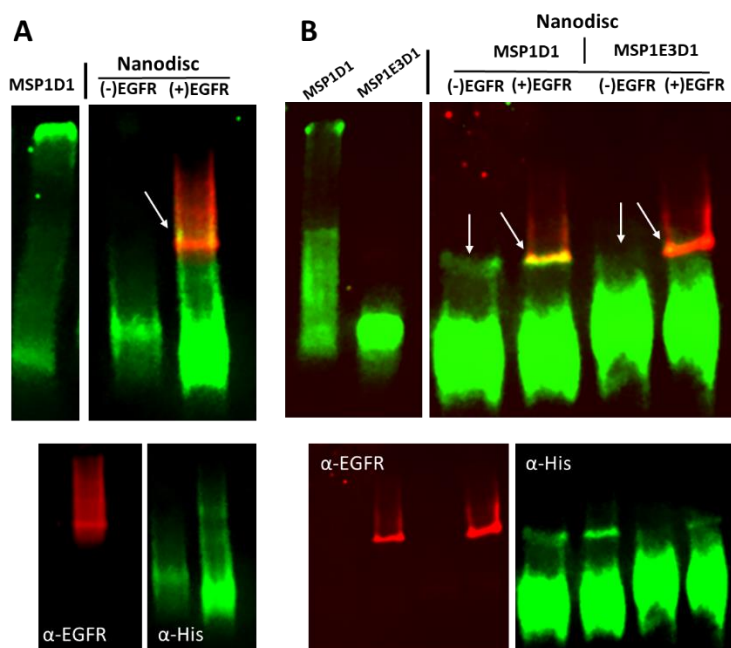## 3.1.4. Optimization of nanodisc size and lipid composition

Figure 8. Native western blot of EGFR-incorporated MSP1D1 and MSP1E3D1 nanodiscs. **A.** Native-PAGE of MSP1D1-DMPC assembled nanodiscs. MSP1D1 (1st lane - green) is run, along with empty nanodiscs (2nd lane - green), as a control to compare changes triggered by assembly. Loaded nanodiscs can be seen in lane 3 and expected colocalization (yellow) between MSP1D1 (green) and EGFR (red) can be seen. Single color blots are shown below. **B.** Comparison between MSP1D1 and MSP1E3D1-assembled nanodiscs on a Native western blot. MSP1E3D1 (2nd lane – green) is a longer protein based on MSP1D1 (1st lane – green). In the native gel, the difference in their mass and charge can be observed. MSP1D1 nanodiscs (lane 3 and 4 – green) present a band (arrow) that runs at a similar height as EGFR (4th lane – red), causing possible false positive colocalization (4th lane – yellow). MSP1E3D1 nanodiscs (lane 5 and 6) do not present a similar band, preventing false positives on native western blots. Single color blots are shown below.

One of the main purposes of this study is to assemble nanodiscs with EGFR and RON heterodimers. Nanodiscs of a larger diameter may better incorporate these heterodimers. Therefore, we tested a larger size of MSP belt protein to form nanodiscs with a larger diameter. MSP1E3D1, an extended version of MSP1D1 with helices 4, 5, and 6 repeated (Bayburt and Sligar, 2010), was used for these experiments. MSP1E3D1 nanodiscs show a single empty nanodisc band, unlike the MSP1D1 empty nanodiscs preparations which would sometimes show a secondary higher band. Because this band was similar to the size of the incorporated nanodisc, overlap could result in a false positive colocalization (**Figure 8B**).

Next, we optimized the phospholipid composition of the nanodiscs. Based on molecular dynamics studies by collaborator César López Bautista (Los Alamos National Laboratory), phospholipids with short carbon-chains, such as DMPC, may not be ideal for transmembrane receptor embedding. Lipids with longer carbon-chains may provide optimal embedding of the transmembrane domain based on nanodisc height and transmembrane domain length. We tested two phospholipid preparations, EggPC and POPC. POPC is a 16
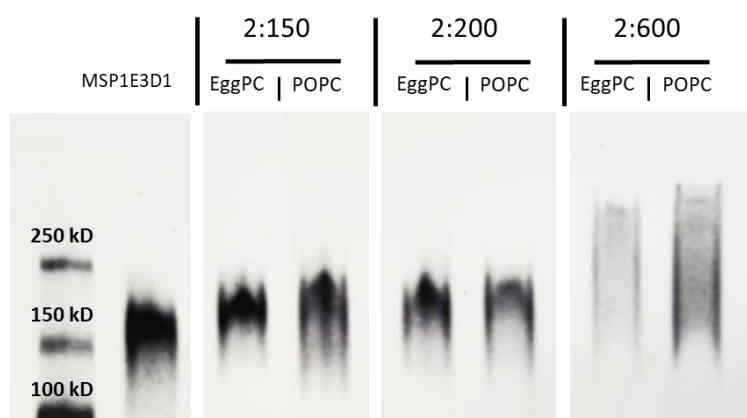
Figure 9. Phospholipid species and ratio analysis in MSP1E3D1 assembled nanodiscs. MSP1E3D1 nanodiscs were assembled with different ratios of phospholipids to find optimal conditions. Nanodiscs containing 150 to 200 phospholipid molecules were successfully assembled with no major differences visible in Native-PAGE. Nanodiscs with 600 lipid molecules tended to form higher molecular weight aggregates.

carbon-chain saturated phospholipid. EggPC is a natural lipid mixture of mainly POPC, but with low levels of cholesterol and sphingomyelin, providing a more native-like lipid bilayer. Several MSP to phospholipid ratios (2:150, 2:200, and 2:600) were tested for nanodisc assembly. Upon nanodisc assembly the higher molecular weight band shown by MSP1D1 was not present in MSP1E3D1 nanodisc assemblies (**Figure 8B**). Assembled empty nanodiscs were seen with both POPC and EggPC. Since a natural lipid mixture such as EggPC would act similar to a native-like membrane, we chose to use EggPC to embed our membrane proteins. The optimal ratio for assembly was 2:150-200 MSP1E3D1 molecules to EggPC phospholipid molecules. This can be

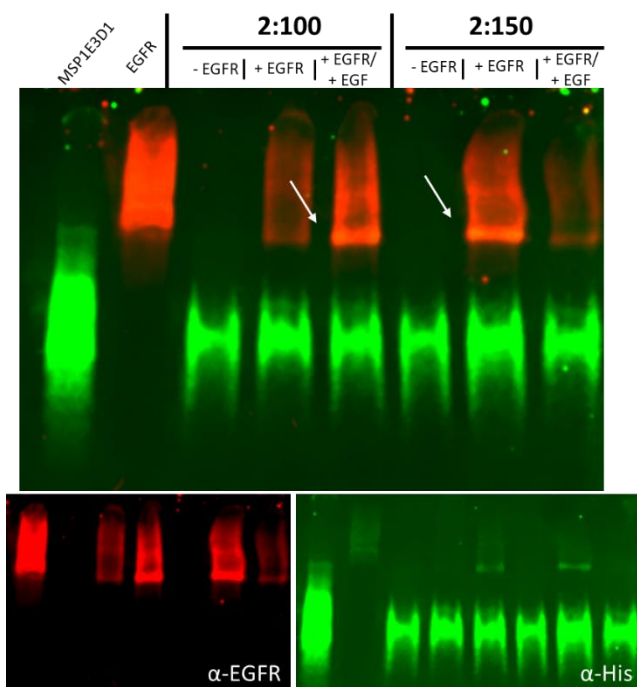seen in **Figure 9**, based on the tightness of the assembled nanodisc bands on the native-PAGE for 2:150-200 (Lanes 2 – 6) belt protein to lipid ratios. A sample with a 2:600 MSP1E3D1 to EggPC or POPC ratio was prepared as a negative control for nanodisc assembly. Bao et al., 2012 suggests that lipid-rich assemblies such as these tend to form aggregates. Based on the native-PAGE in **Figure 9** (lanes 6 and 7), we concluded

Figure 10. Native electrophoresis and fluorescent western blotting of MSP1E3D1-EggPC assembled nanodiscs (+/-) EGFR and EGFR dimers. MSP1E3D1-EggPC nanodiscs were assembled at 2:100 and 2:150 MSP belt protein to Lipid ratio. Purified EGFR from Expi293F cells was added to the nanodisc mixture. EGFR was stimulated with a 2x of EGF for 10 min to form dimers prior to adding to the mixture. In this western blot, colocalization is visible in 2:100 nanodiscs with EGFR dimers, as well as 2:150 nanodiscs with single EGFR protein. This shows that dimer incorporation is dependent on lipid molecules per nanodisc.

that at this MSP to lipid ratio, the size of the nanoparticles produced is not homogeneous.

The next step was to assemble nanodiscs with embedded EGFR. Approximately 1 µM of EGFR was used per sample preparation. To encourage the formation of EGFR dimers, 2 µM of EGF was added to the purified EGFR before adding the protein to the nanodisc mixture. Nanodiscs were assembled overnight by removing the detergent. **Figure 10** shows our results. Nanodisc assembly using a 2:100 MSP to lipid ratio shows overlapping of EGFR and the assembled nanodiscs bands, showing embedded

nanodiscs with EGF-bound EGFR. The sample with a 2:150 MSP to lipid ratio also shows overlapping bands for untreated EGFR and assembled nanodiscs. This means that there is a fraction of nanodiscs that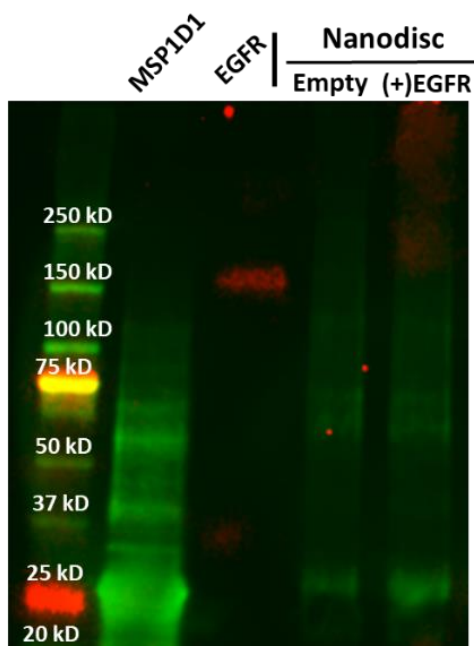 have unliganded EGFR monomers embedded in them. A sample with fewer lipid molecules per nanodisc potentially provides the necessary space to embed dimeric EGFR. This phenomenon needs to be further explored.

EGFR incorporation into our nanodiscs was displaying low efficiencies and protein loses. For further optimization, we examined whether the protein is being lost during nanodisc formation. Nanodisc assembly is triggered by detergent removal. Detergent can be removed using dialysis or adsorption using macroporous polymeric beads or BioBeads. It has been suggested (Franz Hagn et al., 2018) that the membrane protein of interest may bind to the Biobeads yielding a low number of loaded nanodiscs. To test if the yield of EGFR-embedded nanodiscs (**Figure 10**) was low due to the target protein aggregating and binding to the BioBeads, we added denaturing sample buffer to the beads to remove any residual proteins non-specifically bound to the BioBeads. These samples were

Figure 11. Fluorescent western blot of denatured BioBeads after overnight detergent removal for nanodisc assembly. MSP1E3D1 was used as a control and was loaded according to the amount used for nanodisc assembly. An EGFR only control was added to the BioBeads for overnight detergent removal, as well as an empty nanodisc and a loaded nanodisc samples. The BioBeads were denatured by boiling using reducing buffer to remove any protein bound. As seen on Lane 3 and 4, there is some minor nanodisc residue, however EGFR residue is almost undetectable on lane 4. The EGFR only control on lane 2 also shows a very small amount of residue. This experiment shows that protein losses are not likely due to aggregation and attachment to the BioBeads during assembly.

analyzed by fluorescent western blotting for His-tag and EGFR to detect residual MSP1E3D1 and target protein, respectively (**Figure 11**). Some nanodisc residue remains on the beads after overnight detergent removal. However, the BioBeads contained very little EGFR bound as shown by the nearly undetectable EGFR band (Lane 4). An EGFR only control was added to the BioBeads and was incubated overnight with rotation. As seen on **Figure 11** – lane 2, this control also presented a very faint band of EGFR bound to the beads. We concluded that protein losses were not likely due to aggregation and binding to the beads.

3.2. Nanodisc protein incorporation detection methods

Because native electrophoresis and western blotting analysis was sometimes difficult to interpret, we wanted to establish an alternative method for determining protein incorporation into nanodiscs that would allow us to distinguish loaded nanodiscs from empty nanodiscs. Detection methods tested include size exclusion chromatography, imaging techniques, and biochemical assays.

3.2.1. Size exclusion chromatography

Previous nanodisc studies have used size exclusion chromatography to purify loaded nanodiscs from empty nanodiscs or free receptor (Mi et al., 2008; Bayburt and Sligar, 2010; Hagn et al., 2018). Therefore, we tried this detection method on the MSP1E3D1 - EggPC samples using a small-scale agarose-based size exclusion chromatography column (Superdex 200 Increase 10/300). We compared our

nanodisc assembly samples to a series of gel filtration calibration standards, ranging from 29 kDa to 700 kDa (**Figure 12**). These standards were used to approximate the molecular weight of our eluted nanodiscs, and controls based on their elution time. Given this information, our empty nanodiscs assembled with MSP1E3D1 and EggPC have an approximate molecular weight of 150 kDa, which is within what is expected according to the literature (Bayburt and Sligar, 2010). Our loaded nanodiscs eluted at around 19 min. According to our standards the loaded nanodiscs would have a molecular weight of around 400 kDa. This matches our approximation based on the receptor (175kDa) and the nanodisc (150kDa) molecular weights added together.
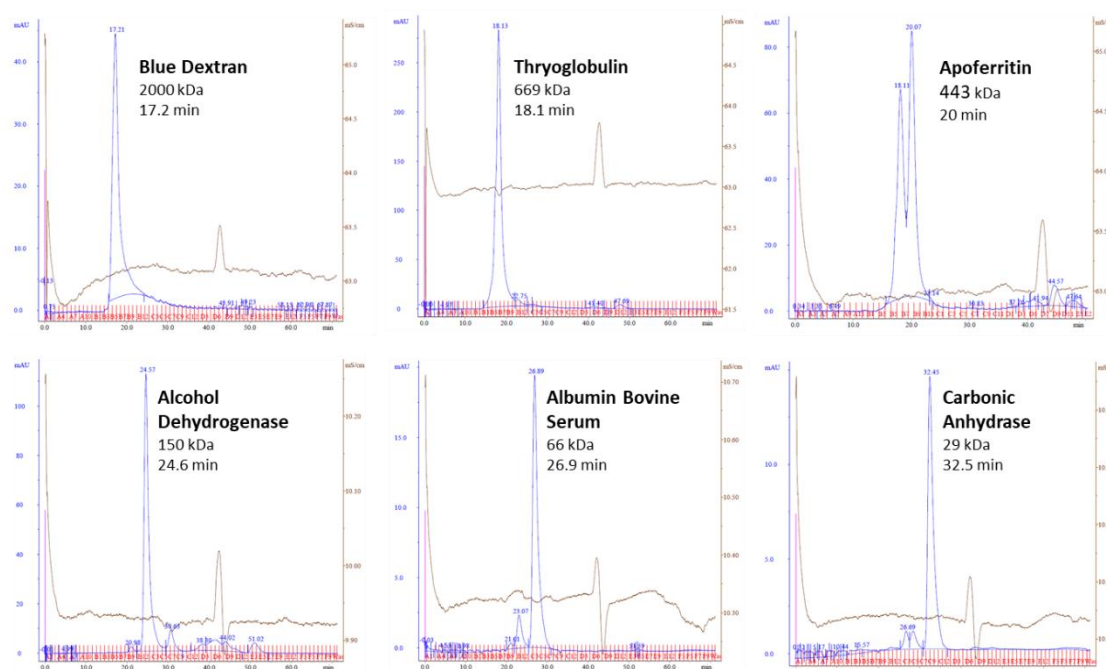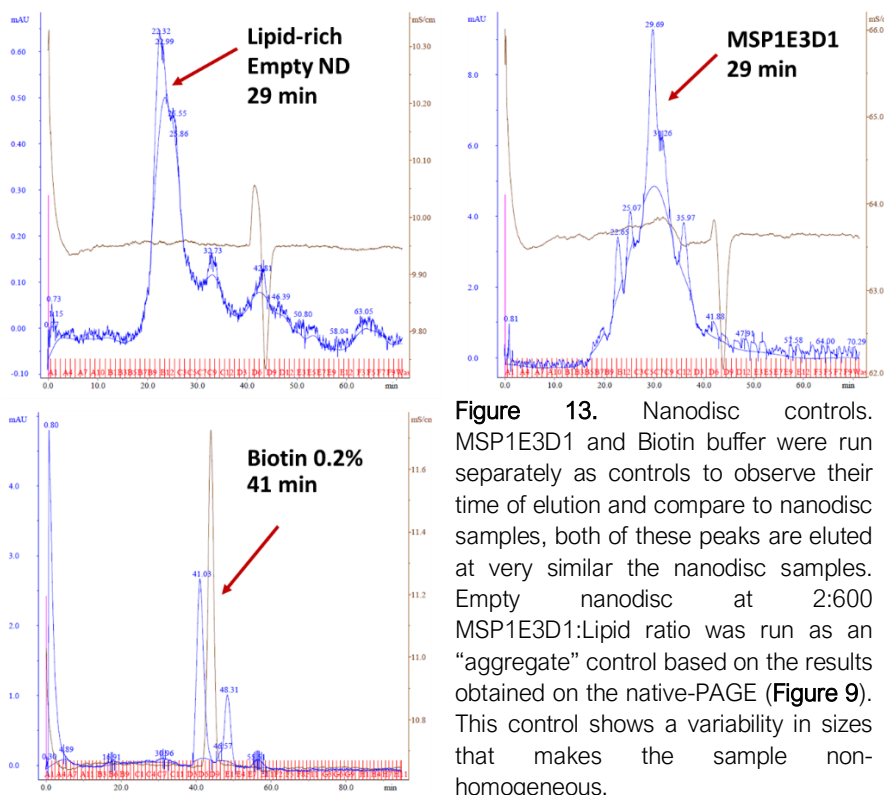

Figure 12. Size exclusion standards ranging from 669 kDa to 29 kDa, and Blue Dextran at 2000 kDa. These standards were run on the same size exclusion column before any nanodisc samples. The elution time of these standards was used to approximate the molecular weight of the eluted nanodiscs and controls

Figure 13. Nanodisc controls. MSP1E3D1 and Biotin buffer were run separately as controls to observe their time of elution and compare to nanodisc samples, both of these peaks are eluted at very similar the nanodisc samples. Empty nanodisc at 2:600 MSP1E3D1:Lipid ratio was run as an "aggregate" control based on the results obtained on the native-PAGE (**Figure 9**). This control shows a variability in sizes that makes the sample non-homogeneous.

A series of controls were run separately on the size exclusion column to observe their peaks and elution time (**Figure 13**). MSP1E3D1 has a representative peak at 29-30 min. This peak appears at the same time on empty and loaded nanodisc samples, indicating that some free MSP belt protein is in solution. The 4mM biotin buffer was also run to confirm that the late peak at 40-41 min was due to the buffer. A third control of empty nanodiscs with an MSP to lipid ratio of 2:600 was run as "aggregates" based on the results obtained by electrophoresis in **Figure 9.** These empty nanodiscs with an excess amount of lipid molecules form lipid-rich molecules that show a variability in sizes. In this nanodisc "aggregate" control, the spectrum obtained shows a very broad distribution in sizes.

Loaded nanodiscs have a distinct peak at 19.6 minutes that corresponds to a molecular weight of 400 kDa (**Figure 14A**). Based on the calculated molecular weight
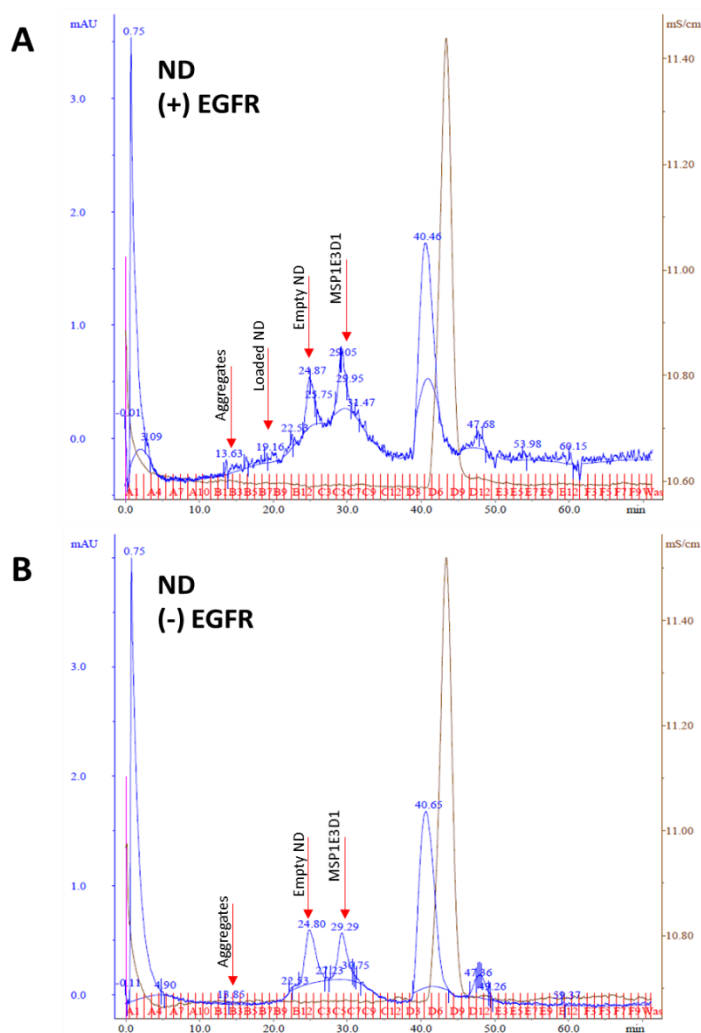
Figure 14. Size exclusion chromatography of empty and loaded nanodiscs. **A.** Loaded nanodiscs show around 19.6 – 20 min. **B.** Empty nanodisc spectrum shows no peak at 19 – 20 min. Empty nanodiscs show at 24 min, and aggregates at 13 min. MSP1E3D1 shows in both spectra at around 29 min.

of the nanodisc and the receptor, this peak is likely the loaded nanodisc. This peak is not visible in empty nanodisc samples (**Figure 14B**). The peak around 30 min or 32 kDa corresponds to the belt protein, based on the MSP1E3D1 control seen in Figure 12. The peak at around 24 min is likely the empty nanodisc since it is present in both assemblies (**Figure 14B**). During elution, 500 µL fractions were collected. Fractions associated with each visible peak were analyzed by SDS-PAGE and western blotting. Unfortunately, no bands were visible, suggesting that the fractions collected were too dilute to detect. Further concentration using low MWCO centrifugal concentrators did not improve the detection.

3.2.2. Affinity precipitation: His-tag PullDown

Figure 15 A. REVERT total protein staining of blotted samples from His-tag affinity precipitation using Ni-NTA resin. A. His-tagged MSP1E3D1 with and without His-tag pulldown (Lane 1 and 2). Comparison between no treatment (lane 3) and His-tag pulldown (lane 4) of emp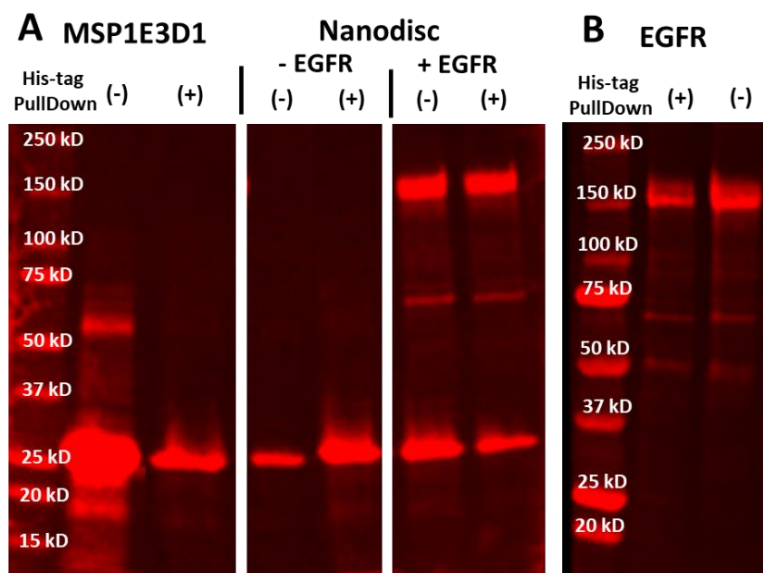ty nanodiscs. Loaded nanodiscs with FL-EGFR showing presence of EGFR on pulldown samples (lane 6). B. EGFR His-tag pulldown indicating EGFR non-specific binding to Ni-NTA resin.

According to the literature, isolation of loaded nanodiscs can be performed through affinity precipitation by using a specific tag on the embedded protein (Bayburt and Sligar, 2010; Hagn et al., 2018). In our case, we used affinity precipitation of the His-tag coupled with SDS-PAGE as a detection method of target protein embedding into nanodiscs. Ni-NTA agarose resin was used to pull-down nanodiscs with the 6x His-tagged MSP1E3D1. A series of controls were used, including empty nanodiscs as a positive control for pull-down, and purified EGFR as a negative control. Complexes bound to the Ni-NTA resin were denatured by boiling and analyzed by SDS-PAGE to identify the proteins that were captured on the resin. The gel membrane was stained with REVERT total Protein Stain (Licor - 926-11010) to detect the proteins (**Figure 15**).

A visible band at 150 kDa showed that EGFR was present in the assembled MSP1E3D1 – EggPC nanodisc pull-downs. A negative control of EGFR only at a

similar concentration as the one used for nanodisc preparation was also pulled-down using Ni-NTA resin. This control showed that EGFR itself was binding to the Ni-NTA resin (**Figure 15A**), making it impossible to distinguish between EGFR embedded in nanodiscs and EGFR bound non-specifically to the Ni-NTA resin. This experiment was repeated using an EGFR only control, with similar results to those observed previously (**Figure 15B**). Pull-down conditions will need to be optimized to limit non-specific binding of EGFR perhaps through further stringent washes. Alternatively, cobalt beads can also bind His-tagged proteins with fewer risk of non-specific binding.

3.2.3. EGFR Immunoprecipitation

Given the non-specific binding of EGFR to the Ni-NTA resin, we attempted pull-down of EGFR-loaded nanodiscs by immunoprecipitating EGFR. To do this, we tested a series of controls on agarose resin conjugated with α-EGFR (clone R-1) antibody. The controls included free EGFR, free MSP1E3D1, and empty nanodiscs. These controls were tested before trying any loaded nanodiscs to observe if any MSP1E3D1 or assembled nanodiscs would non-specifically bind to the α-EGFR conjugated resin. The bound complexes were was denatured by boiling and analyzed by SDS-PAGE and REVERT total protein staining. The results can be seen in **Figure 16.** The first two lanes show MSP1E3D1 and EGFR as non-IP controls. The following 6 lanes show the IP for each control and unbound protein or complex on the supernatant after overnight binding. In the EGFR control, we see EGFR binding to the resin. The MSP1E3D1

control shows low non-specific binding to the α-EGFR conjugated resin with most of

the belt protein remaining

in the supernatant after

binding. Despite these

favorable results, the

empty nanodisc control

shows a strong band for

MSP1E3D1, indicating

that the empty nanodisc

is bound to the resin.

There could be some

interactions between the

conjugated resin and the
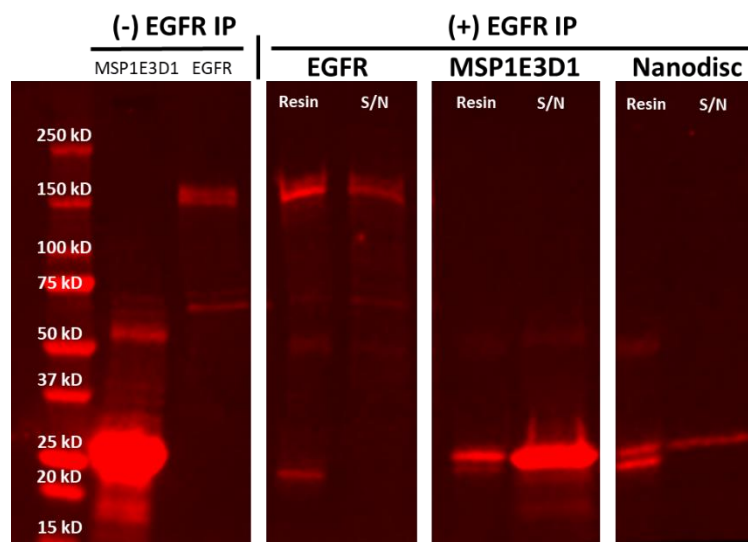
Figure 16. REVERT total protein staining of EGFR immunoprecipitation using agarose beads conjugated with α-EGFR (clone R-1). During this IP, we tested several controls before attempting nanodisc IP via embedded EGFR. The resin was denatured by boiling. The supernatant (S/N) or unbound sample was also loaded on the gel to test for losses or unspecific binding. Lane 1 and 2 show MSP1E3D1 and EGFR that did not undergo IP. Lane 3 and 4 show IP of EGFR FL. Lane 4 shows MSP1E3D1 unspecific binding to α-EGFR conjugated beads. Lane 6 shows unspecific binding of assembled empty nanodiscs to the resin as well.

lipids that form the nanodiscs. Given these results, we decided that pull-down of

EGFR-embedded nanodiscs with this method would not be feasible since non-

specifically bound nanodiscs could affect our ability to distinguish between loaded

and empty nanodiscs

.

3.2.4. Transmission Electron Microscopy

Given their homogeneity in size, the use of nanodiscs for Electron Microscopy allows

us to acquire higher resolution structures of membrane proteins. Nanodiscs also

prevent aggregation of target proteins while preserving their structure and function. These characteristics make nanodiscs a great tool for structural studies as they provide greater uniformity for membrane protein imaging than liposomes or micelles.

In this work, we used EM and negative staining to observe structural and size differences between loaded and empty nanodisc samples to confirm EGFR embedding. As controls, we used EGFR treated with EGF to promote dimer formation, as well as empty nanodisc samples with excess lipids that are known to form aggregates and complexes of varying sizes. The grids were negatively stained using uranyl formate and SBP-tagged EGFR was labelled with streptavidin nanogold. The acquired images were analyzed to obtain average size of the nanodiscs, as well as height and length of EGFR receptors.

Figure 17 shows EM micrographs of the negatively stained samples. EGFR treated with EGF in a number of different orientations can be seen in **Figure 17A**. These negative stain images show two densities of globular appearance that could be the extracellular and kinase domains of EGFR (**Figure 17A**, indent). These two densities are connected by a single-pass transmembrane domain that has a smaller density and is perpendicular to the ECD. Lipid-rich empty nanodisc samples with an MSP to lipid ratio of 2:600 were imaged using EM as a control for aggregates (**Figure 17B**). This sample shows larger aggregates with a wide distribution in size and a general circular appearance. The appearance of this sample matches our results obtained through size-exclusion chromatography and native-PAGE, where these samples appear to have complexes that are non-homogeneous in size. **Figure 17C**

corresponds to empty nanodiscs with an MSP to EggPC ratio of 2:150. This sample has a homogeneous nanodisc size with a distinctive circular appearance and hollow center, similar to those reported by Raschle et al., 2016. These images are in accordance with the results obtained through native-PAGE, western blotting, and size exclusion chromatography, where nanodiscs of a 2:150 – 200 MSP belt protein to lipid ratio appear to have a defined size that varies within a certain margin. This can be seen in the distinct nanodisc elution peak in size-exclusion spectra, and in the defined bands for nanodisc assembly in the native-PAGE and western blotting. Finally, loaded nanodiscs with EGF-treated EGFR were imaged using negative staining and EM (**Figure 17D**). This sample has nanodiscs with an MSP belt protein to lipid ratio of 2:150 and contains empty nanodiscs as well as loaded nanodiscs with dimeric and monomeric EGFR. This diversity in the sample can be observed in the variability of size and different structures that may correspond to protein orientation in nanodiscs embedded with dimeric or monomeric EGFR as well as free EGFR protein. For this sample, SBP-tagged EGFR was labelled using streptavidin nanogold. The inset on **Figure 17D** shows EGFR labelled with streptavidin gold embedded in a nanodisc with a distinct "circular" shape representing the nanodisc, and two separate densities on each side for the ECD and KD of embedded EGFR. A selection of potentially loaded nanodiscs is displayed in **Figure 17E**. These complexes show a number of different shapes, which suggests a variability in structures associated with the number of receptors in the nanodisc, protein orientation, and nanodisc orientation.

Images from TEM were analyzed based on their width and length of several structures identified. These measurements were averaged (**Figure 18**). The lipid-rich empty nanodiscs (**Figure 18A**), had an average of all measurements of 14.2 nm (n=32), which is larger than the expected size for MSP1E3D1 assembled nanodiscs. The measurements for these lipid-rich nanoparticles are shown in **Table 1.** The histogram corresponding to these aggregates **(Figure 18A)** shows a wide range of nanodisc sizes, which is in accordance to previous size-exclusion and native-PAGE results, as well as what can be observed in the EM images. In comparison to these lipid-rich particles, empty nanodiscs of an MSP to lipid ratio of 2:150 (**Figure 18B**) display a defined size and less variability based on the histogram. These nanodisc display an average of 12.4 nm through all measurements (n=31). This corresponds well with the average diameter of 12.1 nm for nanodiscs formed with MSP1E3D1 belt protein as previously described (Denisov et al., 2004). Width and length averages for this sample can be seen in **Table 1.** EGFR dimer samples (no nanodisc) were analyzed and compared to published data from Mi et al., 2011. Based on the literature, the average measurements for EGFR dimers are 10 nm wide and 20 nm long. Our measurements indicate an average width of 10.5 nm and length of 20.9 nm for structures in the EGFR dimer samples (**Figure 18C**). The histogram for these measurements shows a bimodal distribution, where the first normal distribution corresponds to width and the second to length. EGFR loaded nanodiscs on **Figure 18D** display a broad distribution. The average length for this sample is 19.8 nm (n=48), similar to the average length of EGFR dimers. The average width for the loaded nanodiscs is 13.9 nm, a measurement

that is larger than that of empty nanodiscs. In short, the average for both width and length, lies between that of the nanodisc diameter and EGFR dimer length, while length matches EGFR dimer data and width is slightly larger than empty nanodiscs. This variability in distribution and larger than expected width suggests that the loaded nanodisc sample may contain a complex mixture of different species, such as EGFR monomers, EGFR dimers, nanodiscs with embedded EGFR monomers or dimers, as well as interactions between nanodiscs and EGFR monomers without proper embedding.

Table 1. TEM image analysis based on measurements of width and length

Transmission Electron Microscopy - Image Analysis		Mean Size (nm)		
Sample	N	All Measurements	Length	Width
EGFR dimers	32	15.6656	20.8739	10.4573
Lipid-rich empty nanodisc – 2:600	32	14.2181	14.5288	13.9074
Empty nanodisc – 2:150	31	12.4083	13.0933	11.7233
EGFR dimer loaded nanodisc – 2:150	48	16.9976	19.8779	13.9252
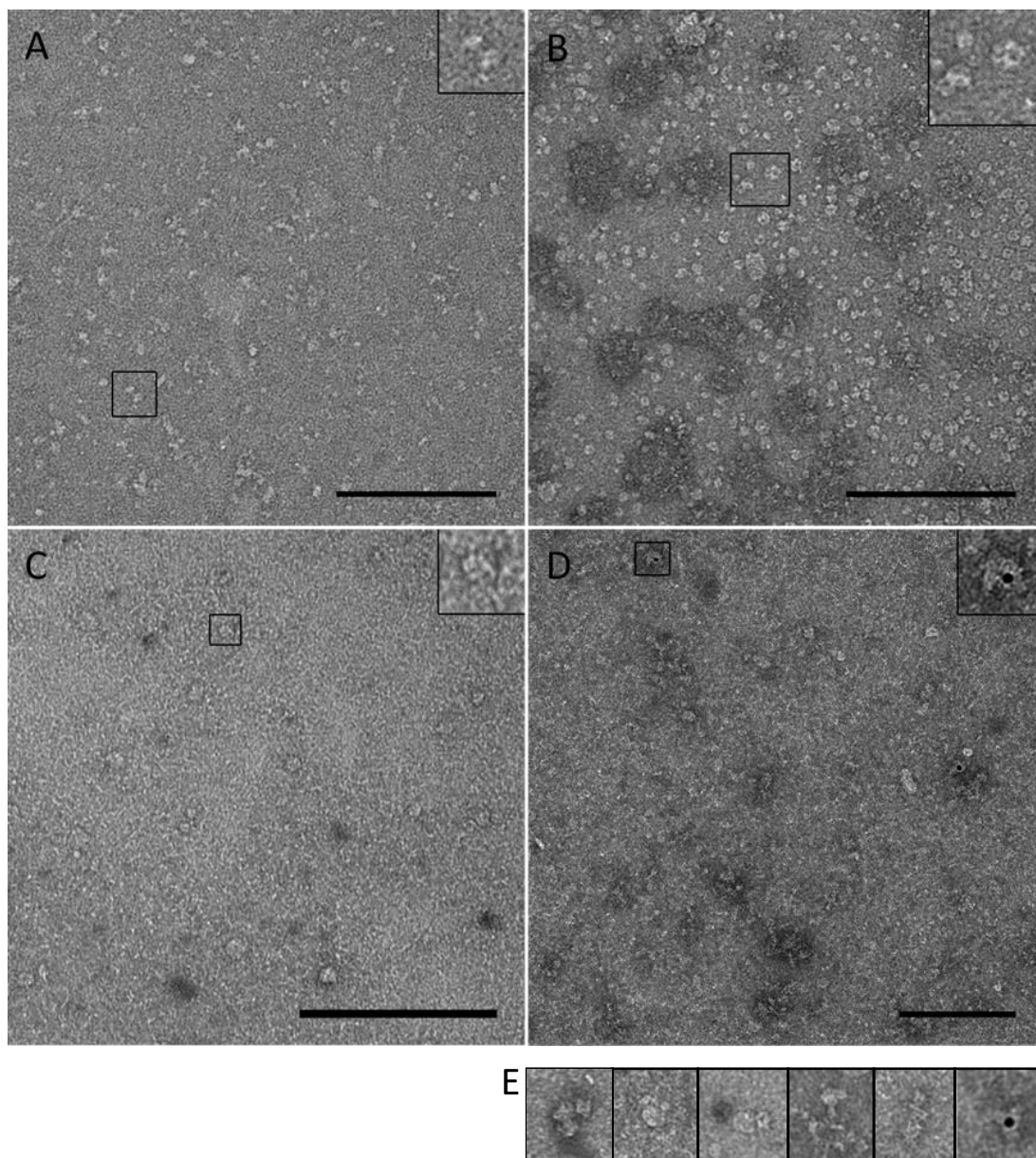
Figure 17. Transmission electron micrographs of negatively stained proteins and nanodiscs. **A.** EGFR + EGF proteins in all orientations; the inset is a possible EGFR dimer. **B.** Empty nanodiscs composed of MSP1E3D1:EggPC 2:600. Note dense aggregates (dark) and nonhomogeneous size of nanodiscs, as indicated by the inset. **C.** Empty nanodiscs composed of MSP1E3D1:EggPC 2:150. The nanodiscs are not aggregated and are more homogenous is size. **D.** EGFR+EGF loaded nanodiscs composed of MSP1E3D1:EggPC 2:150. This sample contains empty nanodiscs, proteins and loaded nanodiscs. The inset displays a nanodisc that is labeled with streptavidin nanogold, indicating the presence of SBP-tagged EGFR. **E.** A selection of potentially loaded nanodiscs. Note the asymmetrical shapes associated with each nanodisc. Scale = 200nm.

Figure 18. Distribution of all measurements for "aggregates", empty nanodiscs, EGFR homodimers, and nanodiscs loaded with EGFR. **A.** Lipid-rich nanodiscs with excess lipids show a broad distribution indicating a wide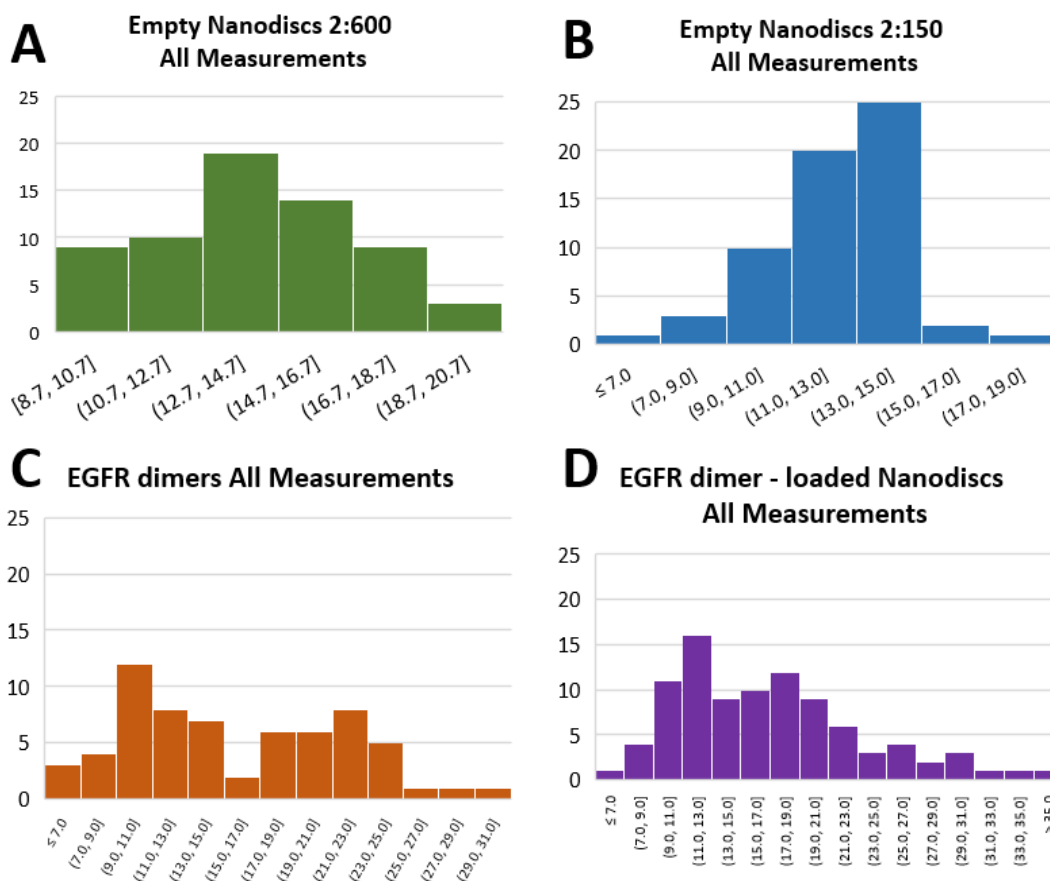 variability in sizes. These results are in accordance with those seen with size exclusion and native western blot. **B.** Empty nanodiscs with an MSP to lipid ratio of 2:150 display less variability in size based on the histogram, with an average diameter of 12.4 nm per nanodisc, which is similar to published diameter of nanodiscs assembled with MSP1E3D1. **C.** EGFR dimer measurements show a bimodal distribution where the first normal distribution corresponds to measurements of width and the second to measurements of length. The average size for these EGFR dimers is 20.9 nm in length and 10.5 nm is width, which is very similar to the measurements published by Mi et al., 2008. **D.** Nanodiscs loaded with EGFR dimers show a broad distribution, which suggests a complex mixture of different structures. The average for all measurements is between that of a nanodisc diameter and EGFR dimer length. The average length of sample matches EGFR dimer data. The average width is slightly larger than empty nanodiscs, and significantly larger than EGFR dimer width.

3.2.5. TIRF imaging of EGFR-nanodisc complexes

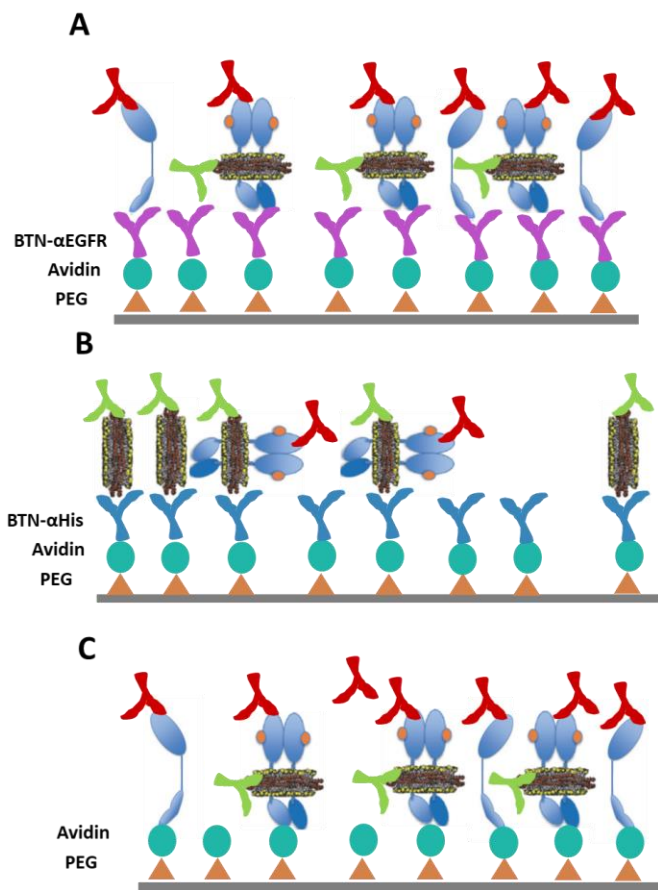Advanced microscopy techniques have been also used to image nanodiscs in assays that involve receptor activation, and controlled nanodisc and protein reconstitution (Lamichhane et al., 2017; Raschle et al., 2015). Lamichhane et al. study conformational transitions of G protein-coupled receptors in nanodiscs using a single molecule assay based on nanodisc assembly with 5% biotinylated lipids that bind a coverslip treated with neutravidin. In our work, we propose a different approach based on coverslip functionalization through neutravidin and biotinylated antibodies followed by pull-down of nanodisc complexes using the

Figure 19. SiMPull array functionalization for single-nanodisc imaging. Nanodiscs were labelled after pulldown using α-His AF488 (green) and α-EGFR AF647 (clone R-1) (red). A. biotinylated α-EGFR glass (purple) functionalization to pulldown EGFR-embedded nanodiscs. The use of PEG (orange) and Avidin (light blue) allows for perfect orientation of biotinylated α-EGFR. B. PEG and Avidin orient a biotinylated α-His tag antibody (blue) on functionalized glass. This arrange allows for pulldown of His-tagged MSP belt proteins surrounding empty and EGFR-embedded nanodiscs. C. Use of NeutrAvidin as a direct pull-down method for SBP-tagged EGFR.

His-tag on the MSP belt protein or the SBP-tag on the embedded receptor. These bound complexes are then labelled using dyes or fluorescently conjugated antibodies

and imaged using Total Internal Reflection Microscopy (TIRF). An assembled nanodisc with embedded receptors should show colocalization of receptor and nanodisc to single molecule spots imaged on the surface of the coverslip. In this study we focused on efficient surface functionalization that allowed nanodisc pull-down via embedded EGFR or MSP belt protein with subsequent detection of receptor and nanodisc using fluorescently-conjugated primary antibodies.

We used standard SiMPull techniques (Salazar-Cavazos et al., 2018) to functionalize 2x2 arrays. These arrays were functionalized using a mixture of Biotin-PEG and mPEG. Each area on the array was later treated with Neutravidin and a biotinylated antibody. We tested three different ways to bind nanodiscs to the surface, as well as two ways to label the nanodiscs and the embedded protein. Biotinylated antibodies against EGFR were used to pull-down EGFR, or antibodies against the His-tag were used to capture the nanodiscs (**Figure 19A and 19B**). Neutravidin was also tested for direct binding of the SBP-tag on the EGFR full-length receptor (**Figure 19C**). Nanodiscs were labelled in-situ after they were pulled down. Initially, DiD (642 excitation) and α-EGFR XP AF555 were used to label the nanodisc lipid membrane and EGFR, respectively. However, DiD was binding non-specifically to the coverslip and creating a high background in both channels. To avoid lipid dyes usage, α-His AF488 and α-EGFR AF647 (clone R-1) were used instead to label His-tagged MSP1E3D1 and EGFR, respectively.

Empty nanodisc and loaded nanodisc samples were imaged, as well as a series of controls including PEG-treated coverslips, functionalized coverslips with biotinylated

his-tag antibody, pre-assembled empty nanodiscs (Cube Biotech – 26311), and free EGFR on functionalized areas of the array.

Figures 20 – 22 show images of areas with samples and controls on biotinylated α-His-tag coverslips obtained through TIRF microscopy using 488 and 642 lasers. **Figure 20** shows two SiMPull functionalization controls for biotinylated α-His pull-down. **Figure 20A** corresponds to two separate areas within the same control sample, a PEG functionalized coverslip with no α-His-tag functionalization. This control provided information on the general noise to expect per area based on PEG treatment. There are a few low intensity spots, particularly on the 642 channel, indicating background autofluorescence from PEG treatment. **Figure 20B** corresponds to a coverslip after α-His functionalization with no sample added. The image shows some low intensity spots in the 642 channel, which can be attributed to the coverslip treatment background fluorescence.

We tested purified EGFR (monomers), as well as pre-assembled MSP1D1 empty nanodiscs from CubeBiotech (**Figure 21**). **Figure 21A** shows two different areas of biotinylated α-His functionalized coverslip with free EGFR as a control. α-EGFR Af647 signal can be observed on the 642 channel corresponding to EGFR on the bottom of the coverslip, which could occur due to non-specific binding or neutravidin affinity pull-down of SBP-tagged EGFR. Compared to the other controls, high density and signal can be observed in the 642 channel, while the 488 channel shows very low noise. **Figure 21B** corresponds to pre-assembled MSP1D1 nanodisc samples from CubeBiotech on an α-His functionalized coverslip. These nanodiscs are assembled

with two 6x his-tagged MSP belt proteins, which should bind to the biotinylated α-His antibody and are then labelled with α-His AF488. The images show that pull-down through this antibody is not highly efficient. However, defined spots of bright signal are visible on the 488 channel and are likely nanodiscs. Despite the fact that the 642 channel shows some fluorescence, there is no colocalization visible between any of the nanodiscs and the signal on the 642 channel. Therefore, this unexpected fluorescence on the 642 channel can be attributed to the coverslip functionalization.

Given this information from the controls, we expected some noise in the 642 channel for the empty and loaded nanodisc samples in **Figure 22**. **Figure 22A** shows empty nanodiscs of a 2:150 MSP to lipid ratio on α-His -functionalized coverslip. Pull down efficiency is not high, which yields a small amount of visible nanodiscs, this could directly relate to the α-His antibody used for pulldown or could also be due to degradation of the nanodisc sample, given the presence of liposomes visible in solution. A higher amount of unexpected signal on the 642 channel can be observed, but after image analysis none of this signal colocalizes with the observed nanodiscs. This unexpected signal on the 642 channel can be attributed to coverslip functionalization or potential nonspecific binding of the α-EGFR Af647 fluorescent antibody. **Figure 22B** corresponds to two areas of an α-His functionalized coverslip with EGF-treated EGFR-loaded nanodiscs. Again, pull down efficiency is rather low, which yields a small number of visible nanodiscs. However, one of the main differences between this sample and the empty nanodisc sample is that a large number of defined spots are present in the 642 channel, which indicates a high

presence of EGFR. As with the EGFR only control, this could happen due to affinity pull-down of SBP-tagged EGFR by available neutravidin sites. This large amount of EGFR indicates that the majority of the target protein in the sample is not getting incorporated into nanodiscs. This could be solved by assembling nanodiscs using a smaller amount of lipid molecules to increase the space for the receptor within the nanodisc, thereby increasing embedding efficiency. Moreover, **Figure 22B** shows colocalization of EGFR and His-tagged MSP1E3D1 in the 642 and 488 channels, respectively (marked by arrows on the merged image). This colocalization indicates EGFR embedding in these nanodiscs.
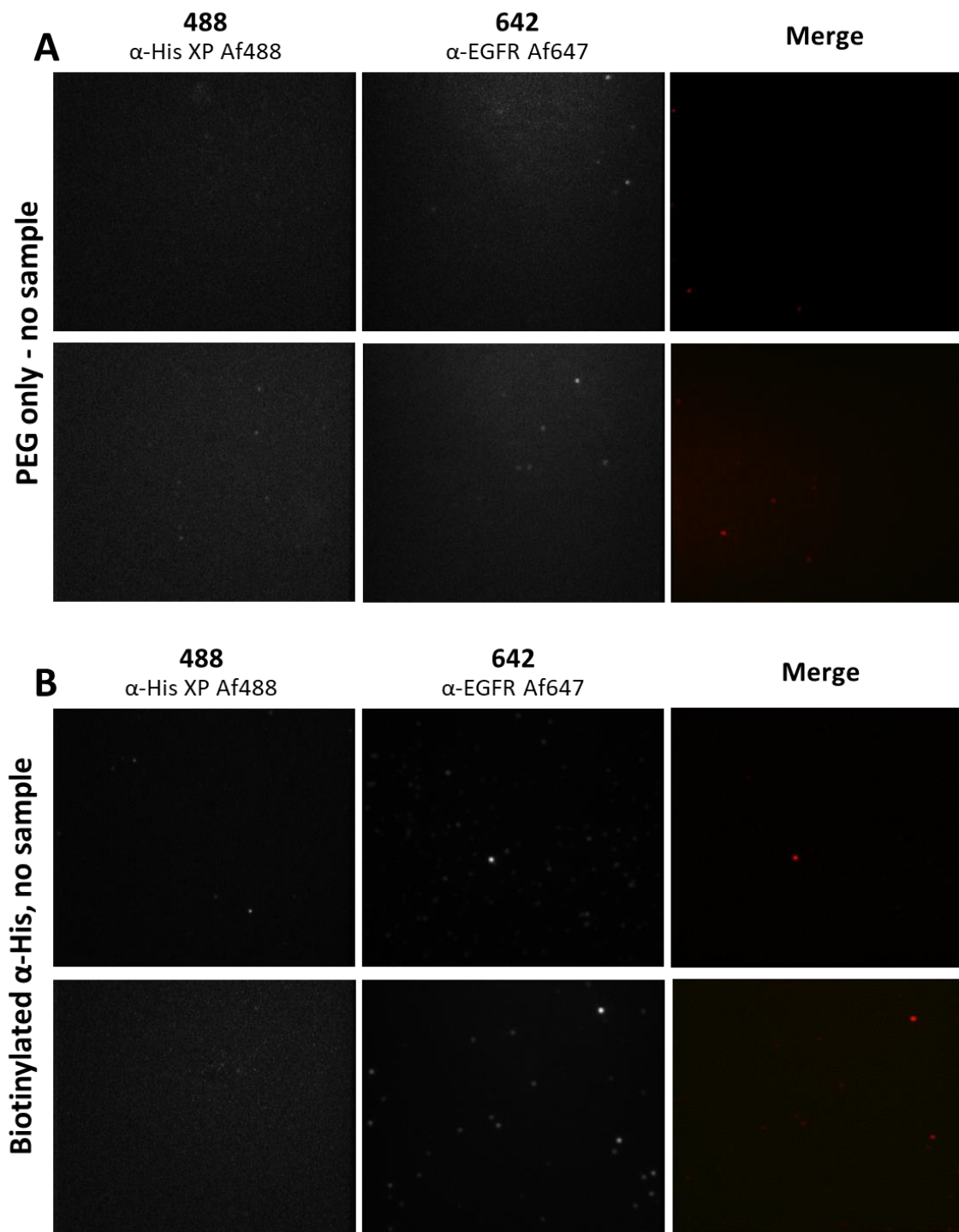
Figure 20. Single-nanodisc imaging controls for biotinylated α-His functionalization. **A.** PEG-only functionalized coverslip shows general low intensity background autofluorescence from PEG treatment. **B.** α-His functionalized coverslip shows noise on the 642 channel of low intensity attributed to treatment.
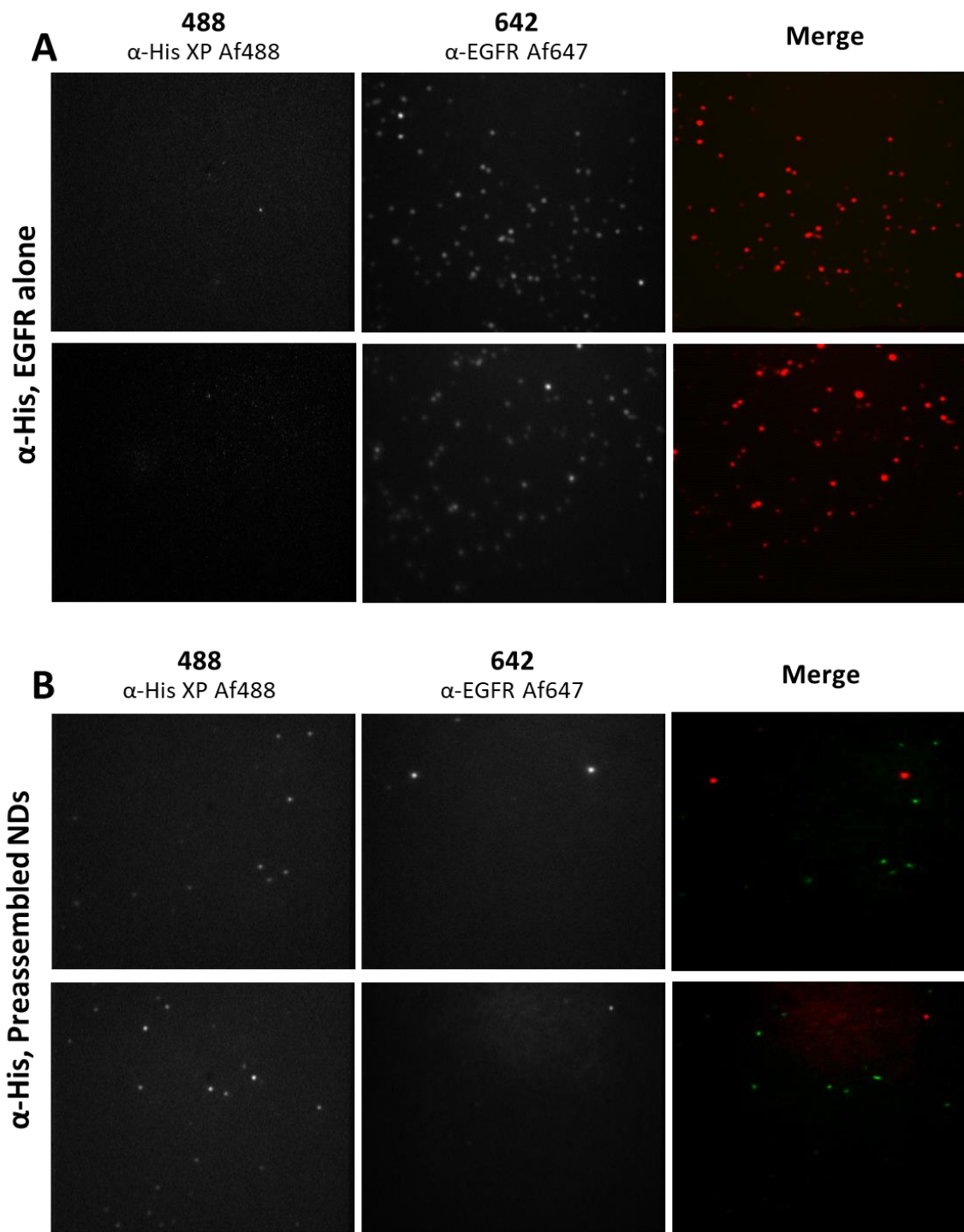
Figure 21. Single-molecule imaging of EGFR monomers and pre-assembled MSP1D1 empty nanodiscs. **A.** α-His functionalized coverslip with free EGFR labelled with α-EGFR Af647. EGFR can be observed on the 642 channel due to neutravidin affinity pull-down of SBP-tagged EGFR. **B.** α-His functionalized coverslip with pre-assembled MSP1D1 nanodiscs from CubeBiotech labelled with α-His AF488. Low density of nanodiscs visible indicates that pull-down is not highly efficient. Unexpected signal on the 642 channel shows no colocalization with the nanodiscs and the signal on the 642 channel.
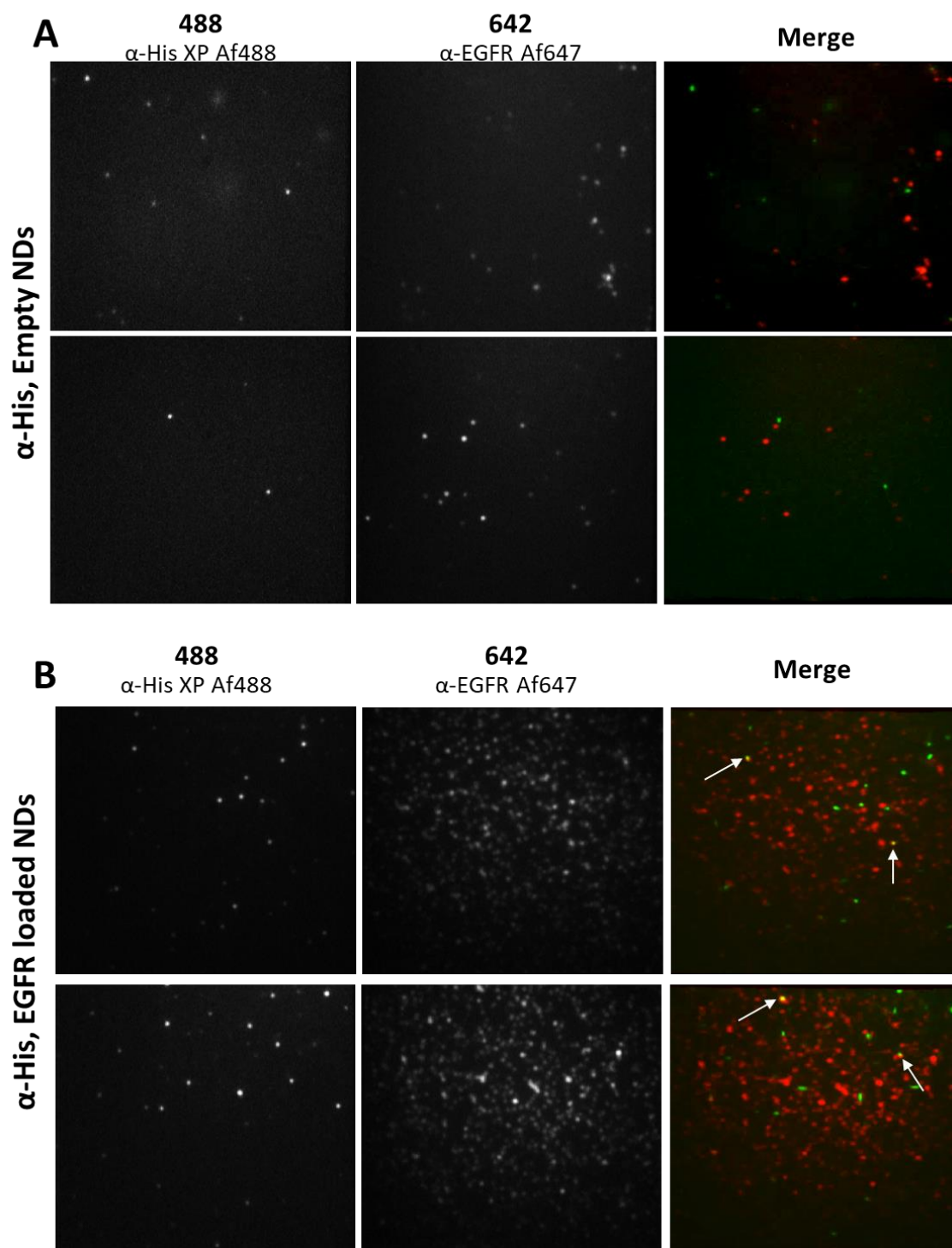
Figure 22. Single-nanodisc imaging of empty and loaded nanodiscs **A.** Empty nanodiscs at a 2:150 MSP1E3D1 to EggPC ratio pulled down using biotinylated α-His antibody. Low pulldown efficiency could be due to degradation of the nanodisc sample. More noise in the 642 channel is visible, but none colocalizes with the nanodiscs. **B.** Nanodiscs loaded with EGFR dimers. A small number of nanodiscs is visible in the 488 channel. High numbers of EGFR are visible in this sample possibly due to affinity pull-down of the SBP-tag by neutravidin. Colocalization within the two channels is marked by arrows, suggesting the presence of EGFR-embedded nanodiscs.

CHAPTER 4: CONCLUSIONS

Membrane receptors are responsible for a series of signaling pathways that are directly related to basic cell functions. These pathways are triggered by mechanisms whose structure is not fully understood. Protein structural studies provide information that reveals the structure-function relationship behind receptor interactions. Through this work, we focused on two RTKs that are expressed in different tissues and are responsible for a number of cell functions, EGFR and RON. EGFR is a membrane receptor that regulates cell functions, such as apoptosis, migration, proliferation, and differentiation. RON is a membrane receptor of the MET family that is responsible for cell migration and proliferation. Both of these receptors have been shown to play a role in cancer. Although the structure and consequence of EGFR homodimerization have been extensively studied, there is evidence of crosstalk between EGFR and other receptors, including RON, that is less explored. Aberrant trans-activation of RON and EGFR due to crosstalk has been related to tumorigenesis, and although these two receptors have been shown to co-immunoprecipitate, the structural information behind this interaction remains unknown.

Protein structural studies are imperative to fully understand the function behind these receptor interactions. However, these studies are oftentimes difficult to achieve due to protein solubilization, which is key to maintaining target proteins in a functional state. There are a few techniques to solubilize membrane proteins, which include the use of detergents that form detergent-protein micelles and the use of lipid vesicles. However, these techniques often interfere with a number of assays and optical

techniques, reduce protein activity, and may lead to denaturation. Nanodisc are an excellent tool for structural studies, providing a native-like environment of homogeneous size to embed membrane proteins that prevents aggregation and maintains the receptor's conformation and functionality.

This work focused on developing a nanodisc assembly protocol to achieve embedding of full-length RON and/or EGFR, as well as finding alternative methods for detection of embedded nanodiscs.

Nanodiscs have been used before to solubilize a number of proteins, including EGFR. Our first aim was to optimize a nanodisc assembly protocol by manipulating nanodisc size and lipid content to allow embedding of EGFR or RON into nanodiscs.

To achieve this, we needed a method to generate enough recombinant protein for nanodisc incorporation. One of the biggest challenges behind the production of functional membrane protein is the need for correct processing of proteins. While bacteria can produce high yields of membrane proteins, it is not uncommon that the proteins produced are not folded properly. Functional membrane proteins are imperative for structure-function studies, and proper processing and folding is only achieved using mammalian cells which generally have a low protein yield. In the beginning of this work, our recombinant target proteins had been expressed in HEK293 cells, and the purification process required further concentration of the eluate, which in turn yielded enough protein for only one nanodisc preparation. This

hindered the possibility to run other controls during each preparation, such as embedding on different MSP-lipid ratios as well as purified EGFR (no nanodisc).

To increase protein yields, we transiently transfected our recombinant proteins in the Expi293F cell line. These cells are HEK293 modified cells that grow in suspension, increasing protein yields. This cell line increased protein production for full length EGFR as well as RON fragments. Initially, full-length RON was not processed correctly through this cell line. This means that RON was unable to properly get cleaved and transported to the membrane. To stop protein translation and thus reduce the concentration of pro-RON in the cells, we treated the cells with CHX, reducing the pro-RON:RON ratio from 1:1 to 1:4 in the lysate.

We based our preliminary studies on previous work by Mi et al 2008, where EGFR is embedded in MSP1D1-DMPC nanodiscs. These experiments appeared to be successful based on native-PAGE results. However, we resolved that given the size of our target receptors, the use of larger nanodiscs could facilitate and perhaps increase receptor embedding. Similarly, based on molecular dynamics modeling studies from collaborators, we concluded that using a lipid with longer carbon chains would increase nanodisc height and potentially be beneficial for proper embedding of the transmembrane domain, as well as helping avoid unwanted interactions between the MSP belt protein and the embedded membrane receptor.

We tested nanodisc assembly using MSP1E3D1, a longer version of MSP1D1, as well as EggPC, a natural lipid mixture of mostly POPC, a 16-carbon chain lipid. To obtain

the optimal MSP to lipid ratio, we tested the assembly of different nanodiscs with an increasing number of lipid molecules per belt protein, including nanodiscs with lipid excess (2:600). It was determined that the optimal MSP:lipid ratio was 2:150. EGFR incorporation was tested on nanodiscs with MSP:lipid ratios of 2:100 and 2:150, where EGFR and EGF-treated EGFR incorporation was observed via native-PAGE in both cases, respectively. Despite these results, it was clear that complementary methods of analysis that would allow us to determine nanodisc embedding were needed.

One of the methods that is commonly described in previous work is size exclusion chromatography. In this case, nanodiscs assemblies are run through a size exclusion column that separates loaded from empty nanodiscs, as well as raw components, such as MSP belt protein and target protein, that have not been incorporated. Size exclusion chromatography provided information regarding EGFR incorporation into nanodiscs by showing distinct peaks for empty and embedded nanodiscs. However, previous work suggests that the fractions must be recovered and analyzed by SDS-PAGE to obtain definitive information for embedding. In our case, these fractions were too dilute to be detected via western blot.

Since our nanodisc preparations were relatively smaller than those reported by previous work, we attempted to determine a method that would be more suitable to detect nanodisc incorporation in smaller nanodisc assembly preparations. We attempted to use affinity precipitation to pull-down the nanodiscs using the His-tag on the MSP belt protein. After pull-down the resin was denatured and analyzed via SDS-

PAGE. Despite the presence of EGFR in the "loaded" nanodisc samples, we discovered this was due to nonspecific binding of EGFR to the Ni-NTA resin, thus deeming it impossible to determine if the nanodiscs contained receptor or not.

We also tested EGFR immunoprecipitation to pull-down loaded nanodiscs. Similar techniques have been reported in previous work, in which a target protein with a tag is pulled down via affinity. In our case, we used agarose resin conjugated with an EGFR antibody to pull-down on EGFR-embedded nanodiscs. However, our controls showed that despite the good binding of EGFR, there was nonspecific binding of empty nanodiscs to the resin. In our opinion, despite our unfavorable results for affinity precipitation and immunoprecipitation of embedded nanodiscs, this is a method that should be further explored to obtain an approximation of embedded nanodiscs in small preparations.

We used EM and negative staining to image purified EGFR, empty nanodiscs, and loaded nanodiscs to observe any structural differences between the samples that could provide information on nanodisc embedding, as well as general sizes for the structures found within each sample. According to our results, EGFR and EGF-treated EGFR show distinct sizes and structures that are similar to those reported in previous work. Our empty nanodisc assemblies show a homogeneous size and a distinct circular structure and an average diameter of around 12.4 nm, which concurs with the size reported for MSP1E3D1. Our loaded nanodisc samples show a variety of different structures, including empty nanodiscs and non-embedded EGFR. Despite the low yield of loaded nanodiscs some structures appear to be nanodiscs with

embedded protein. Therefore, visual inspection of nanodiscs samples is a useful method for determining the extent of protein incorporation using only a small amount of sample.

An unexpected finding originates from EM imaging of "aggregates" or lipid-rich nanodiscs of 2:600 MSP-lipid ratio. These excess-lipid complexes display the appearance of larger nanodiscs of heterogeneous size. This poses an interesting question regarding the organization of the MSP belt protein that allows it to associate with other MSPs to generate longer MSP- complexes that surround a larger amount of lipids.

We also tested protocols for single molecule imaging of nanodisc-EGFR complexes. To achieve this, we functionalized the surface of coverslips with neutravidin to prompt the correct orientation of biotinylated antibodies through affinity. These antibodies were used to pull-down either His-tagged MSP belt proteins or EGFR. The nanodiscs and receptors were labelled by using fluorescent antibodies. Using TIRF microscopy, we were able to define individual molecules which allowed us to find colocalization between EGFR and the nanodiscs. Finding colocalization allowed us to determine that embedding efficiency was low and that the majority of the EGFR was not incorporated in nanodiscs. This showed us that the EGFR:nanodiscs ratio can be reduced in future preparations, which will use less EGFR protein. Also, it may be helpful to reduce the amount of lipids per nanodisc, as this could provide more "space" for receptors to insert more efficiently.

Through this study we attempted to find new methods to reliably detect nanodisc embedding for smaller preparations. One of the most relevant findings includes the combination of techniques that provide information on nanodiscs quality (EM) and embedding efficiency (single molecule microscopy), while using small sample amounts. The use of these techniques allows to reduce nanodisc "trial and error" that comes with deciphering the number of lipid molecules per MSP based on the size of the target protein.

In conclusion, the techniques used throughout this work are intended to better understand the behavior of nanodiscs and how these self-assembled complexes are affected depending on the size of the target protein to incorporate. In particular, I have 1) established protein purification protocols using the new Expi293 cells that provide a higher yield of protein; 2) determined the proper choice of MSP belt protein and lipid composition for larger transmembrane complexes; and 3) shown that a combination of EM and single molecule imaging provided a useful approach to characterizing nanodisc samples while using a small sample size. This research sets the precedent for the development of techniques that allow us to properly identify and optimize receptor embedding into nanodiscs for further structural studies.

CHAPTER 5: FUTURE DIRECTIONS

Based on the information collected through EM and single-molecule imaging, we found that a high fraction of the EGFR is not being incorporated during nanodisc assembly. This could be due to an excessive amount of lipid molecules per nanodisc, given the fact that upon receptor embedding, these lipid molecules will be displaced by the transmembrane domain. The results suggest that although there are some loaded nanodiscs, the amount of lipid in the nanodisc mixture may not allow the membrane receptor to incorporate due to the lack of space within the nanodisc. It is necessary to go back and attempt nanodisc assembly with a slightly reduced amount of lipid molecules to increase embedding efficiency.

Given the results obtained through affinity precipitation, it is clear that improving this method could make it a great tool to determine receptor embedding. This technique could be easily applied to small nanodisc preparations and would expand on the results obtained through native-PAGE. A possible experiment that could broaden this technique is the use of streptavidin resin for affinity precipitation of SBP-tagged EGFR embedded in nanodiscs. After pull-down, the resin could be denatured by boiling and the supernatant containing the proteins bound could be analyzed by SDS-PAGE, this would help determine target protein incorporation by showing the presence of MSP belt protein along with pull-down EGFR.

Affinity precipitation using streptavidin resin to pull-down on embedded EGFR could provide cleaner samples for imaging. One of the benefits of streptavidin affinity

precipitation is the fact that it involves gentle elution, that is, bound proteins can be eluted from the streptavidin resin without the use of detergents or imidazole that could potentially affect the integrity of nanodiscs. The presence of biotin from the target protein eluate so far has shown no direct effects on nanodisc assembly. Therefore, streptavidin affinity precipitation of EGFR-embedded nanodiscs and consecutive elution using biotin could decrease the number of empty nanodiscs in the sample, thus increasing the probability of finding loaded nanodiscs during single molecule imaging and EM.

The goal of this work was to establish a protocol that would make nanodisc assembly and receptor embedding detection a reliable process for structural studies of membrane proteins. We have determined a work flow for purification of recombinant protein, nanodisc-protein incorporation, and characterization of the nanodisc sample.

Ultimately, this work sets the precedent for future studies in our group of EGFR and RON homodimers and heterodimers within a single nanodisc.

CHAPTER 6: REFERENCES

Bao, H., Duong, F. & Chan, C. S. A Step-by-step Method for the Reconstitution of an ABC Transporter into Nanodisc Lipid Particles. *J. Vis. Exp.* 8–13 (2012). doi:10.3791/3910

Bax, A. TWO-DIMENSIONAL NMR AND PROTEIN STRUCTURE. *Annu. Rev. Biochem.* **58,** 223–256 (1989).

Bayburt, T. H., Leitz, A. J., Xie, G., Oprian, D. D. & Sligar, S. G. Transducin activation by nanoscale lipid bilayers containing one and two rhodopsins. *J. Biol. Chem.* **282,** 14875–14881 (2007).

Bayburt, T. H., Sligar, S. G. & Biology, C. Membrane Protein Assembly into Nanodiscs. *FEBS Lett.* **584,** 1721–1727 (2016).

Benight, N. M. & Waltz, S. E. Ron receptor tyrosine kinase signaling as a therapeutic target. *Expert Opin. Ther. Targets* **16,** 921–931 (2012).

Blume-Jensen, P. & Hunter, T. Oncogenic kinase signaling. *Nature* **411,** 355 (2001).

Bondos, S. E. & Bicknell, A. Detection and prevention of protein aggregation before, during, and after purification. *Anal. Biochem.* **316,** 223–231 (2003).

Borch, J. & Hamann, T. The nanodisc: A novel tool for membrane protein studies. *Biol. Chem.* **390,** 805–814 (2009).

Burgess, A. W. *et al.* An Open-and-Shut Case? Recent Insights into the Activation of EGF/ErbB Receptors. *Mol. Cell* **12,** 541–552 (2003).

Chao, K. L., Gorlatova, N. V., Eisenstein, E. & Herzberg, O. Structural basis for the binding specificity of human recepteur d'origine nantais (RON) receptor tyrosine kinase to macrophage-stimulating protein. *J. Biol. Chem.* **289,** 29948–29960 (2014).

Chen, J. E. & Glover, G. H. HHS Public Access. **25,** 289–313 (2016).

Cheng, H. L. *et al.* Co-expression of RON and MET is a prognostic indicator for patients with transitional-cell carcinoma of the bladder. *Br. J. Cancer* **92,** 1906–1914 (2005).

Cho, H.-S. & Leahy, D. J. Structure of the Extracellular Region of HER3 Reveals an Interdomain Tether. *Science (80-.).* **297,** 1330 LP-1333 (2002).

Cho, H.-S. *et al.* Structure of the extracellular region of HER2 alone and in complex with the Herceptin Fab. *Nature* **421,** 756 (2003).

Choi, W.-S., Rice, W. J., Stokes, D. L. & Coller, B. S. Three-dimensional reconstruction of intact human integrin alphaIIbbeta3: new implications for activation-dependent ligand binding. *Blood* **122,** 4165–4171 (2013).

Danilkovitch-Miagkova, A. & Leonard, E. J. Cross-talk between RON receptor tyrosine kinase and other transmembrane receptors. *Histol. Histopathol.* **16,** 623–631 (2001).

Daury, L. *et al.* Tripartite assembly of RND multidrug efflux pumps. *Nat. Commun.* **7,** 10731 (2016).

Dobreva, I., Fielding, A., Foster, L. J. & Dedhar, S. Mapping the Integrin-Linked Kinase Interactome Using SILAC. *J. Proteome Res.* **7,** 1740–1749 (2008).

Edwards, J. S. *et al.* Multi-Structure Super-Resolution Imaging using DNA Strand Displacement. *Biophys. J.* **114,** 348a (2018).

Efremov, R. G., Leitner, A., Aebersold, R. & Raunser, S. Architecture and conformational switch mechanism of the ryanodine receptor. *Nature* **517,** 39 (2014).

Engelman, J. A. *et al.* MET Amplification Leads to Gefitinib Resistance in Lung Cancer by Activating ERBB3 Signaling. *Science (80-.).* **316,** 1039 LP-1043 (2007).

Faham, N. & Welm, A. L. RON signaling is a key mediator of tumor progression in many human cancers. *Cold Spring Harb. Symp. Quant. Biol.* **81,** 177–188 (2016).

Ferguson, K. M. *et al.* EGFR Ligands Differentially Stabilize Receptor Dimers to Specify Signaling Kinetics. *Cell* **171,** 683–695.e18 (2017).

Finkenwirth, F. *et al.* ATP-dependent conformational changes trigger substrate capture and release by an ECF-type biotin transporter. *J. Biol. Chem.* **290,** 16929–16942 (2015).

Fogen, D., Wu, S. C., Ng, K. K. S. & Wong, S. L. Engineering streptavidin and a streptavidin- binding peptide with infinite binding affinity and reversible binding

capability: Purification of a tagged recombinant protein to high purity via affinity-driven thiol coupling. *PLoS One* **10,** 1–25 (2015).

Franco Nitta, C. *et al.* EGF Activation of EGFR Drives Crosstalk with RON at the Plasma Membrane. *Biophys. J.* **114,** 462a (2018).

Gao, T. *et al.* Characterization of De Novo Synthesized GPCRs Supported in Nanolipoprotein Discs. *PLoS One* **7,** 5–12 (2012).

Garrett, T. P. J. *et al.* Garrett (2003) Crystal structure of a truncated ErbB2 ectodomain reveals an active conformation. **11,** 495–505 (2008).

Gasmi-Seabrook, G. M. C. *et al.* Oncogenic and RASopathy-associated K-RAS mutations relieve membrane-dependent occlusion of the effector-binding site. *Proc. Natl. Acad. Sci.* **112,** 6625–6630 (2015).

Gatsogiannis, C. *et al.* Membrane insertion of a Tc toxin in near-atomic detail. *Nat. Struct. &Amp; Mol. Biol.* **23,** 884 (2016).

Goadsby, P. J., Kurth, T. & Pressman, A. HHS Public Access. **35,** 1252–1260 (2016).

Gogol, E. P. *et al.* Three dimensional structure of the anthrax toxin translocon-lethal factor complex by cryo-electron microscopy. *Protein Sci.* **22,** 586–594 (2013).

Greenbaum, A., Rajput, A. & Wan, G. RON kinase isoforms demonstrate variable cell motility in normal cells. *Heliyon* **2,** (2016).

Hagn, F., Etzkorn, M., Raschle, T. & Wagner, G. Optimized Phospholipid Bilayer Nanodiscs Facilitate High- Resolution Structure Determination of Membrane Proteins. *J. Am. Chem. Soc.* **Accepted M,** 1–7 (2013).

Hagn, F., Nasr, M. L. & Wagner, G. Assembly of phospholipid nanodiscs of controlled size for structural studies of membrane proteins by NMR. *Nat. Protoc.* **13,** 79 (2017).

Her, C. *et al.* The Charge Properties of Phospholipid Nanodiscs. *Biophys. J.* **111,** 989–998 (2016).

Ian, P. R. & Elizabeth, S. A. Cytochrome P450 Protocols. *Cytochrome P450 Protoc.* **1,** 1–12 (2006).

Jares-Erijman, E. A. & Jovin, T. M. FRET imaging. *Nat. Biotechnol.* **21,** 1387–1395 (2003).

Kang, C. M., Babicky, M. L. & Lowy, A. M. The RON Receptor Tyrosine Kinase in Pancreatic Cancer Pathogenesis and Its Potential Implications for Future Targeted Therapies. **43,** 183–189 (2015).

Keefe, A. D., Wilson, D. S., Seelig, B. & Szostak, J. W. One-step purification of recombinant proteins using a nanomolar-affinity streptavidin-binding peptide, the SBP-tag. *Protein Expr. Purif.* **23,** 440–446 (2001).

Kleinschmidt, J. H. *Lipid-protein interactions : methods and protocols*. (2013). doi:10.1007/978-1-62703-275-9

Lai, A. Z., Abella, J. V. & Park, M. Crosstalk in Met receptor oncogenesis. *Trends Cell Biol.* **19,** 542–551 (2009).

Leitz, A. J., Bayburt, T. H., Barnakov, A. N., Springer, B. A. & Sligar, S. G. Functional reconstitution of β2-adrenergic receptors utilizing self-assembling Nanodisc technology. *Biotechniques* **40,** 601–612 (2006).

Lemmon, M. A. & Schlessinger, J. Cell signaling by receptor tyrosine kinases. *Cell* **141,** 1117–1134 (2010).

Lleó, C. & Prinz, M. Consonant clusters in child phonology and the directionality of syllable structure assignment. *J. Child Lang.* **23,** 105–117 (1996).

Lu, C. *et al.* Structural Evidence for Loose Linkage between Ligand Binding and Kinase Activation in the Epidermal Growth Factor Receptor. *Mol. Cell. Biol.* **30,** 5432–5443 (2010).

Lu, Y., Yao, H.-P. & Wang, M.-H. Multiple variants of the RON receptor tyrosine kinase: Biochemical properties, tumorigenic activities, and potential drug targets. *Cancer Lett.* **257,** 157–164 (2007).

Macdonald-Obermann, J., Li, Y., Piwnica-Worms, D., Pike, L. J. & Westfall, C. Quantitation of the Effect of ErbB2 on Epidermal Growth Factor Receptor Binding and Dimerization. *J. Biol. Chem.* **287,** 31116–31125 (2012).

Maggiora, P. *et al.* Overexpression of the RON gene in human breast carcinoma. *Oncogene* **16,** 2927–2933 (1998).

Maruyama, I. Mechanisms of Activation of Receptor Tyrosine Kinases: Monomers or Dimers. *Cells* **3,** 304–330 (2014).

Matthies, D. *et al.* Cryo-EM Structures of the Magnesium Channel CorA Reveal Symmetry Break upon Gating. *Cell* **164,** 747–756 (2016).

Mi, L. Z. *et al.* Functional and structural stability of the epidermal growth factor receptor in detergent micelles and phospholipid nanodiscs. *Biochemistry* **47,** 10314–10323 (2008).

Mi, L. Z. *et al.* Simultaneous visualization of the extracellular and cytoplasmic domains of the epidermal growth factor receptor. *Nat. Struct. Mol. Biol.* **18,** 984–989 (2011).

Mi, L. *et al.* Functional and Structural Stability of the Epidermal Growth Factor Receptor in Detergent Micelles and Phospholipid Nanodiscs Functional and Structural Stability of the Epidermal Growth Factor Receptor in Detergent Micelles and Phospholipid Nanodiscs †. *Biochemistry* 10314–10323 (2008). doi:10.1021/bi801006s

Ortiz-Zapater, E. *et al.* MET-EGFR dimerization in lung adenocarcinoma is dependent on EGFR mtations and altered by MET kinase inhibition. *PLoS One* **12,** e0170798 (2017).

Peace, B. E., Hill, K. J., Degen, S. J. F. & Waltz, S. E. Cross-talk between the receptor tyrosine kinases Ron and epidermal growth factor receptor. *Exp. Cell Res.* **289,** 317–325 (2003).

Periasamy, A. *et al.* Cell-free protein synthesis of membrane (1,3)-β-d-glucan (curdlan) synthase: Co-translational insertion in liposomes and reconstitution in nanodiscs. *Biochim. Biophys. Acta - Biomembr.* **1828,** 743–757 (2013).

Prahallad, A. & Bernards, R. Opportunities and challenges provided by crosstalk between signalling pathways in cancer. *Oncogene* **35,** 1073–1079 (2016).

Regad, T. Targeting RTK signaling pathways in cancer. *Cancers (Basel).* **7,** 1758–1784 (2015).

Sadler, E. E., Kapanidis, A. N. & Tucker, S. J. Solution-Based Single-Molecule FRET Studies of K+ Channel Gating in a Lipid Bilayer. *Biophys. J.* **110,** 2663–2670 (2016).

Schwartz, S. L. *et al.* Differential mast cell outcomes are sensitive to FcεRI-Syk binding kinetics. *Mol. Biol. Cell* **28,** 3397–3414 (2017).

Shaw, D. *et al.* Architecture and membrane interactions of the EGF receptor. *Cell* **152,** 557–569 (2013).

Shenkarev, Z. O. *et al.* Recombinant Production, Reconstruction in Lipid–Protein Nanodiscs, and Electron Microscopy of Full-Length α-Subunit of Human Potassium Channel Kv7.1. *Biochem.* **83,** 562–573 (2018).

Sibilia, M. & Wagner, E. F. Strain-dependent epithelial defects in mice lacking the EGF receptor. *Science (80-.).* **269,** 234 LP-238 (1995).

Skar-Gislinge, N. *et al.* Small-angle scattering determination of the shape and localization of human cytochrome P450 embedded in a phospholipid nanodisc environment. *Acta Crystallogr. Sect. D Biol. Crystallogr.* **71,** 2412–2421 (2015).

Stella, G. M. *et al.* RON tyrosine kinase mutations in brain metastases from lung cancer. *ERJ Open Res.* **4,** 00083-2017 (2018).

Takeuchi, K. & Ito, F. Receptor Tyrosine Kinases and Targeted Cancer Therapeutics. *Biol. Pharm. Bull.* **34,** 1774–1780 (2011).

Ullrich, A. & Schlessinger, J. Signal transduction by receptors with tyrosine kinase activity. *Cell* **61,** 203–12 (1990).

Valley, C. C., Liu, S., Lidke, D. S. & Lidke, K. A. Sequential Superresolution Imaging of Multiple Targets Using a Single Fluorophore. *PLoS One* **10,** e0123941 (2015).

Viennet, T. *et al.* Reconstitution and NMR Characterization of the Ion-Channel Accessory Subunit Barttin in Detergents and Lipid-Bilayer Nanodiscs. *Front. Mol. Biosci.* **6,** 1–12 (2019).

Viennet, T. *et al.* Reconstitution and NMR Characterization of the Ion-Channel Accessory Subunit Barttin in Detergents and Lipid-Bilayer Nanodiscs. *Front. Mol. Biosci.* **6,** 1–12 (2019).

Waltz, S. E. *et al.* Characterization of the mouse Ron/Stk receptor tyrosine kinase gene. *Oncogene* **16,** 27–42 (1998).

Wu, S. C., Wang, C., Hansen, D. & Wong, S. L. A simple approach for preparation of affinity matrices: Simultaneous purification and reversible immobilization of a streptavidin mutein to agarose matrix. *Sci. Rep.* **7,** 1–10 (2017).

Xu, X. P. *et al.* Three-dimensional structures of full-Length, membrane-embedded human alphaIIbbeta3 integrin complexes. *Biophys. J.* **110,** 798–809 (2016).

Xu, X. P. *et al.* Three-Dimensional Structures of Full-Length, Membrane-Embedded Human α ilb β 3 Integrin Complexes. *Biophys. J.* **110,** 798–809 (2016).

Yokoyama, N., Ischenko, I., Hayman, M. J. & Miller, W. T. The C terminus of RON tyrosine kinase plays an autoinhibitory role. *J. Biol. Chem.* **280,** 8893–8900 (2005).

Zocher, M. *et al.* Single-Molecule Force Spectroscopy from Nanodiscs: An Assay to Quantify Folding, Stability, and Interactions of Native Membrane Proteins. *ACS Nano* **6,** 961–971 (2012).